European Materials Research Society 2022 Fall Meeting in Warsaw, Poland
Symposium L: Doping at the nanoscale: new challenges and advanced applications – Monday, September 19th

High-performance passivating contacts for Si PV based on engineered, doped nanopinholes through dielectric layers

Caroline Lima Salles[1,2], William Nemeth[1], Harvey Guthrey[1], Chun-Sheng Jiang[1], Sumit Agarwal[1,2], Paul Stradins[1]

[1]National Renewable Energy Laboratory, [2]Colorado School of Mines, Golden USA

NREL Transforming ENERGY

U.S. DEPARTMENT OF ENERGY
Energy Efficiency & Renewable Energy

COLORADOSCHOOLOFMINES
EARTH • ENERGY • ENVIRONMENT

The U.S. National Renewable Energy Laboratory

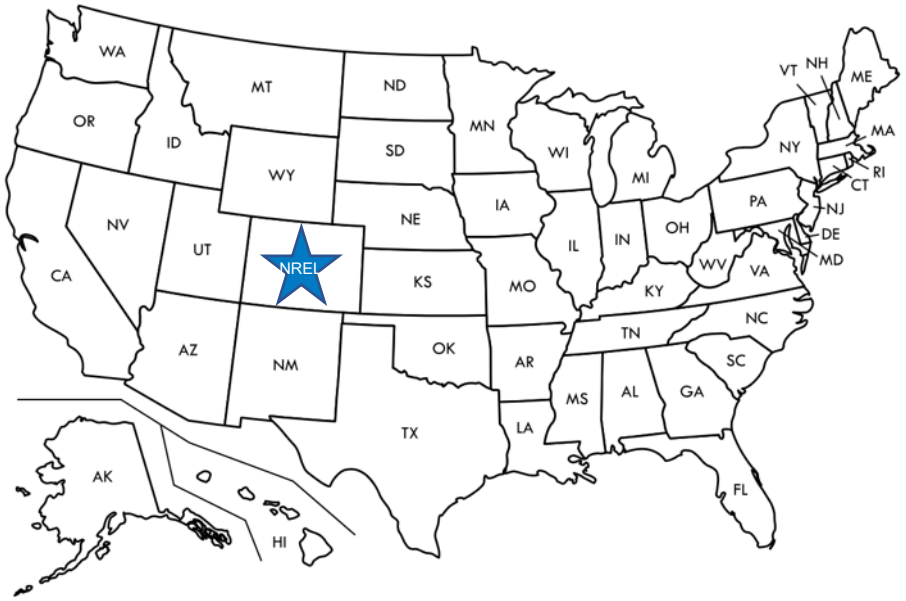

Our campus in Golden, Colorado

R&D Programs

Foundational Science
Materials Science
Biological Systems Science
Computational Science and Visualization

Renewable Power
Solar
Wind
Water
Geothermal

Energy efficiency
Buildings
Advanced Manufacturing

Sustainable Transportation
Bioenergy
Hydrogen and Fuel cells
Vehicles and Transportation Systems

Energy Systems Integration
Energy Storage
Grid modernization
Multipathway Systems Integration

Ref: NREL. “Mission-Focused Materials,” 2022.

Si PV leads the PV world market

Learning curve for module price as a function of cumulative shipments

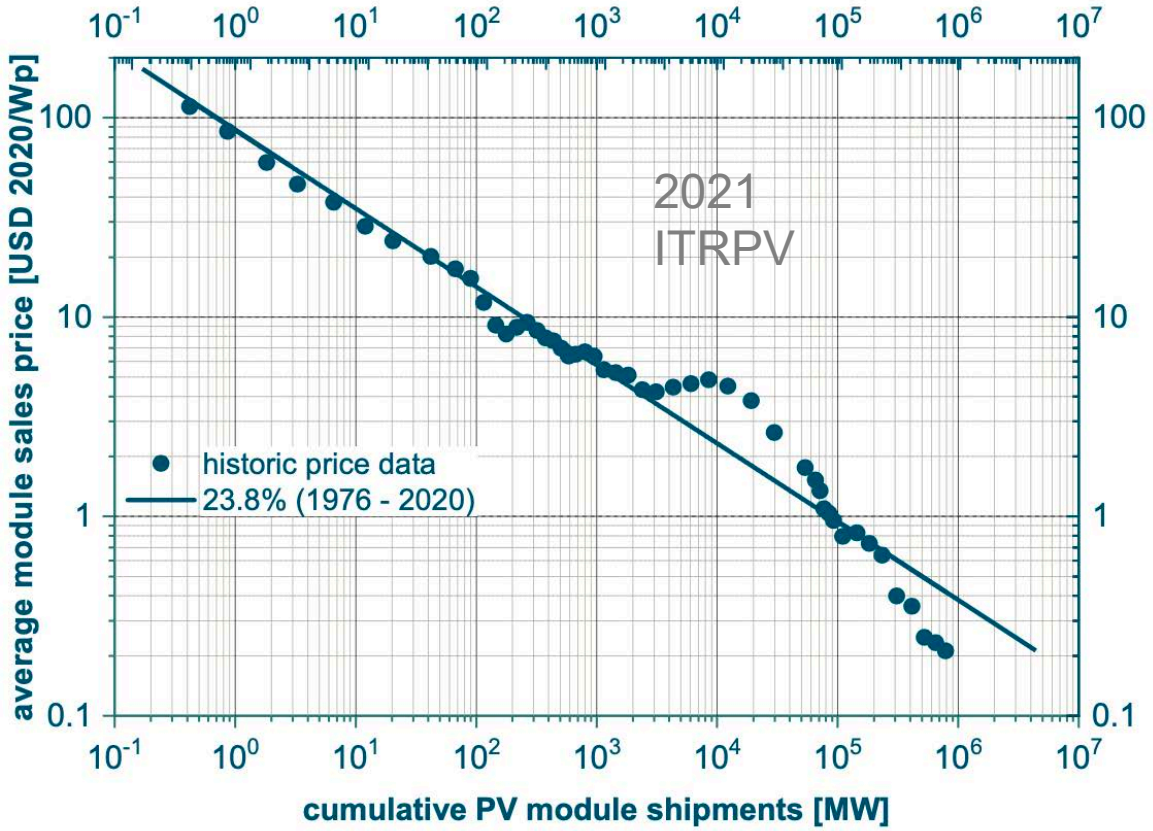

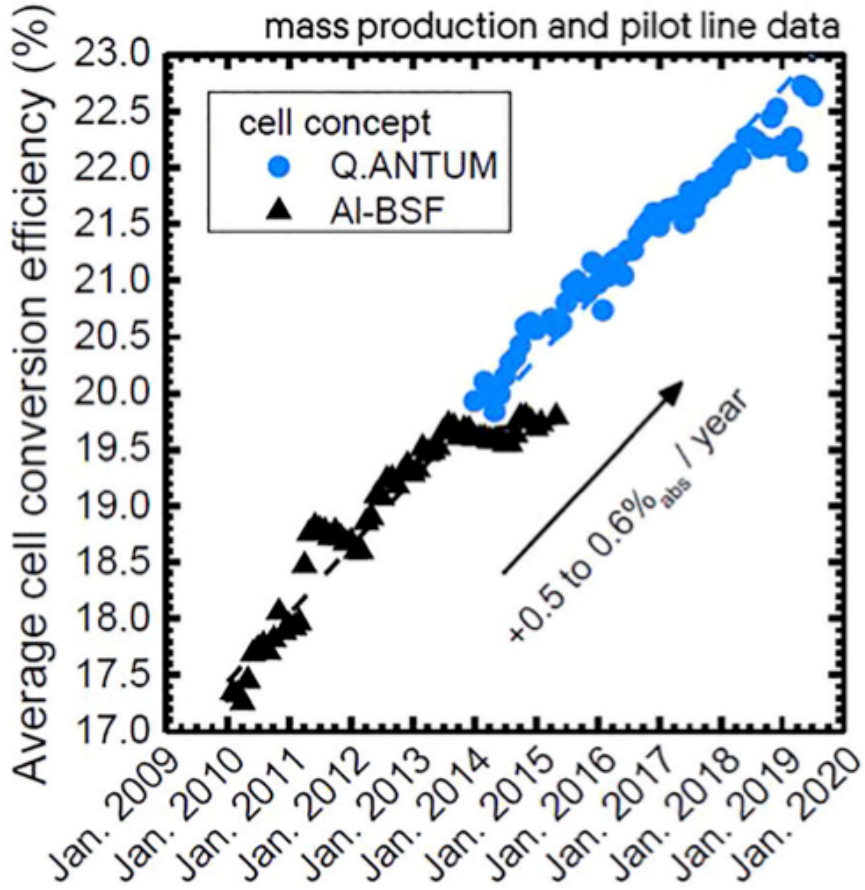

Fertig, F. et al., *2019 AsiaChem*.

Silicon-based solar cells hold 95% of the world market share [2021 ITRPV].

Silicon solar cells: charge-carrier selective contacts

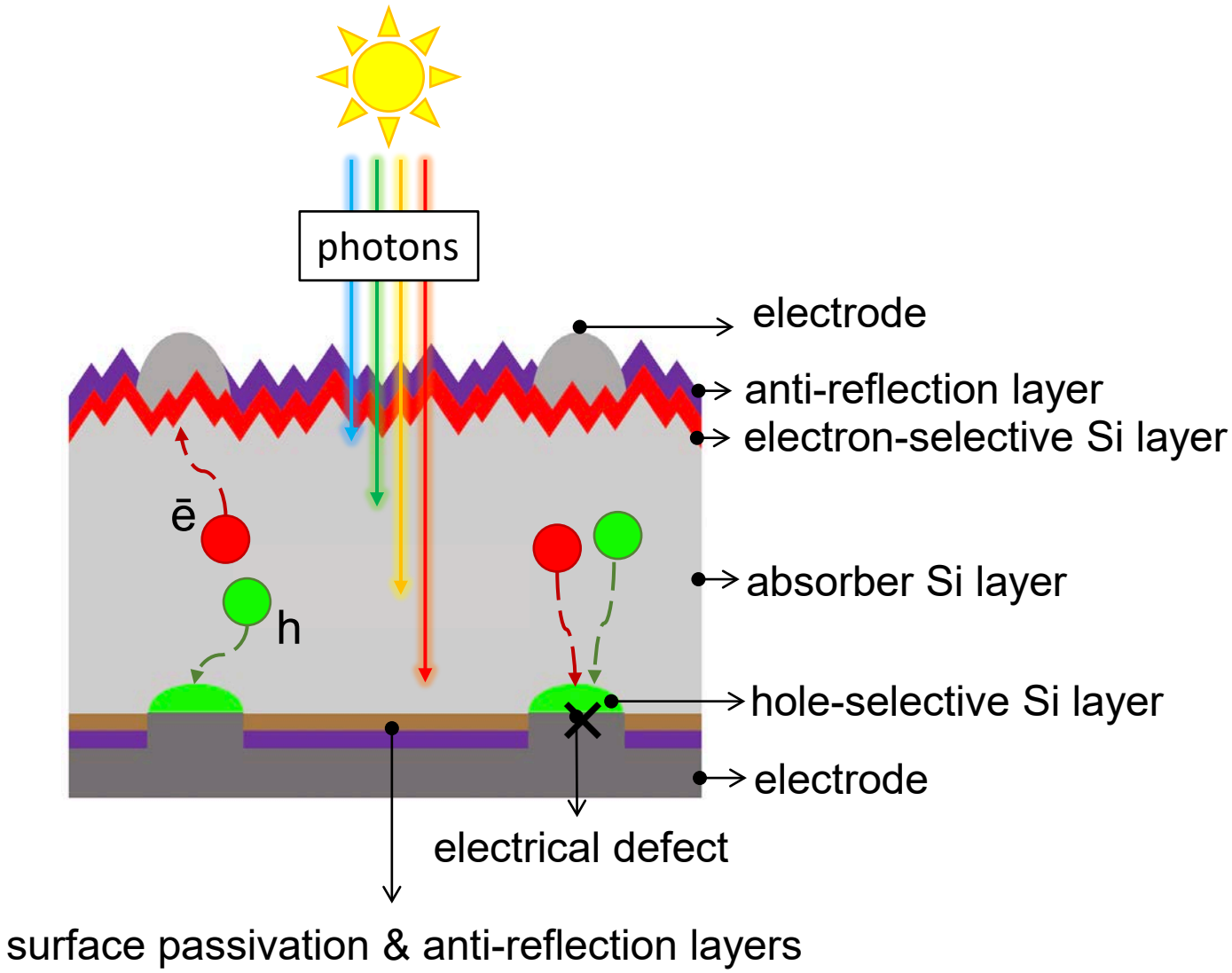

Photons generate electron-hole pairs in the absorber layer

The purpose of texture

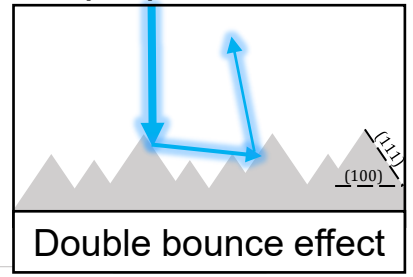

"To achieve the highest possible open circuit voltage, electron-hole recombination must be minimized" [1]

Ideal selective contacts minimize premature electron-hole recombination via *surface defect passivation*

[1] Yablonovitch et al. "A 720 mV open circuit voltage SiOx:c-Si:SiOx double heterostructure solar cell," APL. 1985.

Highly doped *c*-Si confers charge-carrier selectivity, at a cost

PERC: the mainstream industrial cell

The reduced rear contact area minimizes losses due to surface recombination

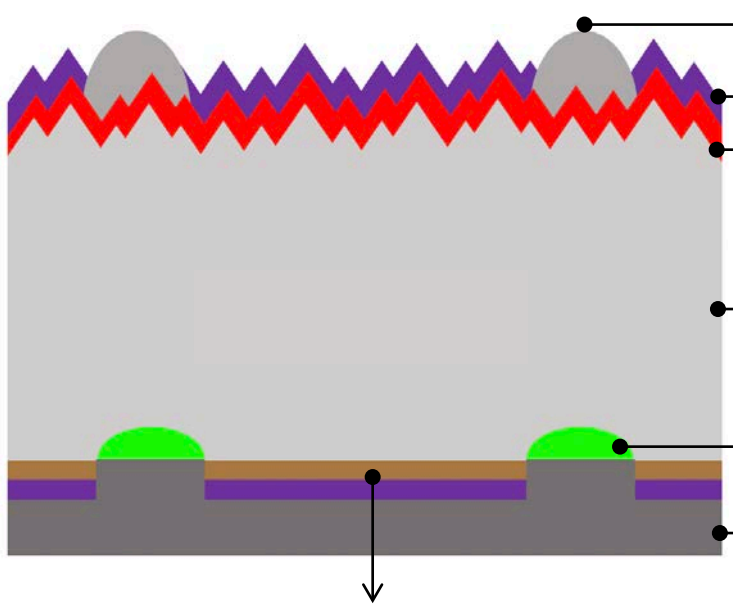

- In n^+ Si, [ē] >> [h], conferring much higher conductivity for ē. The opposite is true for p^+ *c*-Si.
- Higher concentration of dopants in n^+ and p^+ enhances recombination via Auger-Meitner effect.

Surface passivation as a function of rear contact area fraction

The recombination parameter J_0 is commonly used to characterize surface passivation

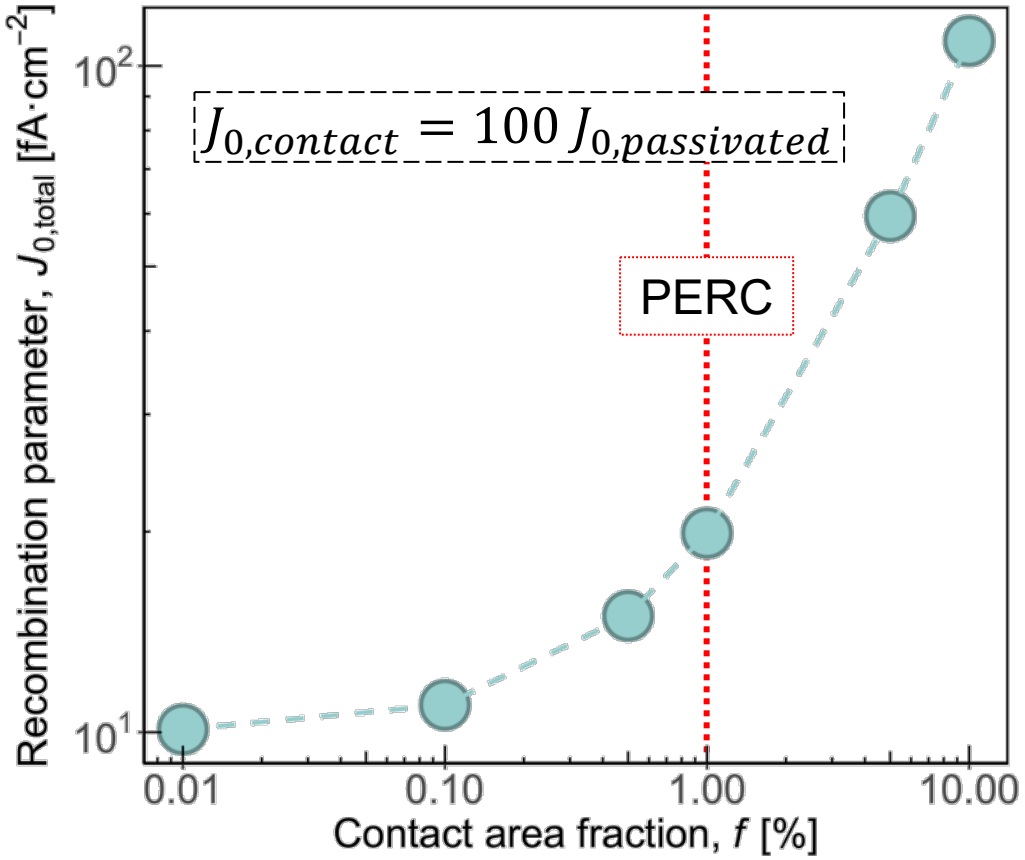

$$J_{0,total} = f \times J_{0,contact} + (1 - f) \times J_{0,passivated}$$

where is f the contact area fraction, ρ_w the wafer resistivity, and r the contact opening radius

Surface passivation & resistivity as a function of rear contact area fraction

The recombination parameter J_0 is commonly used to characterize surface passivation

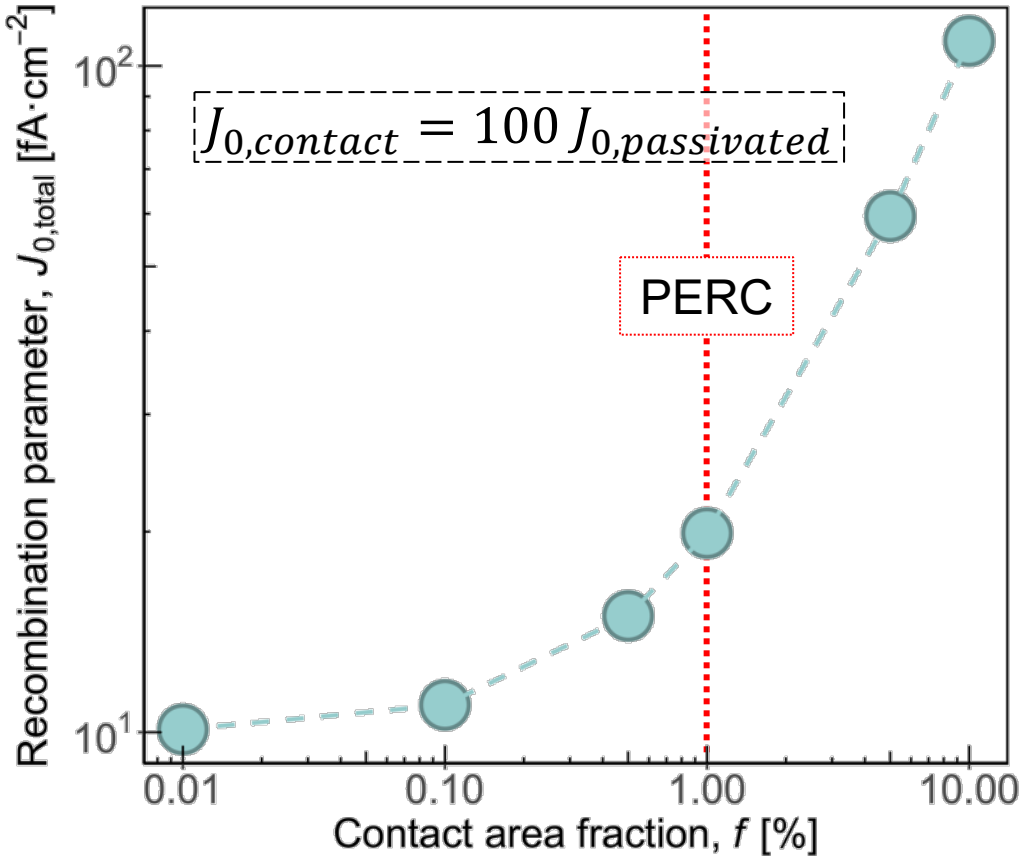

Total contact resistivity approximation where the spreading resistance due to circular openings [1] dominates

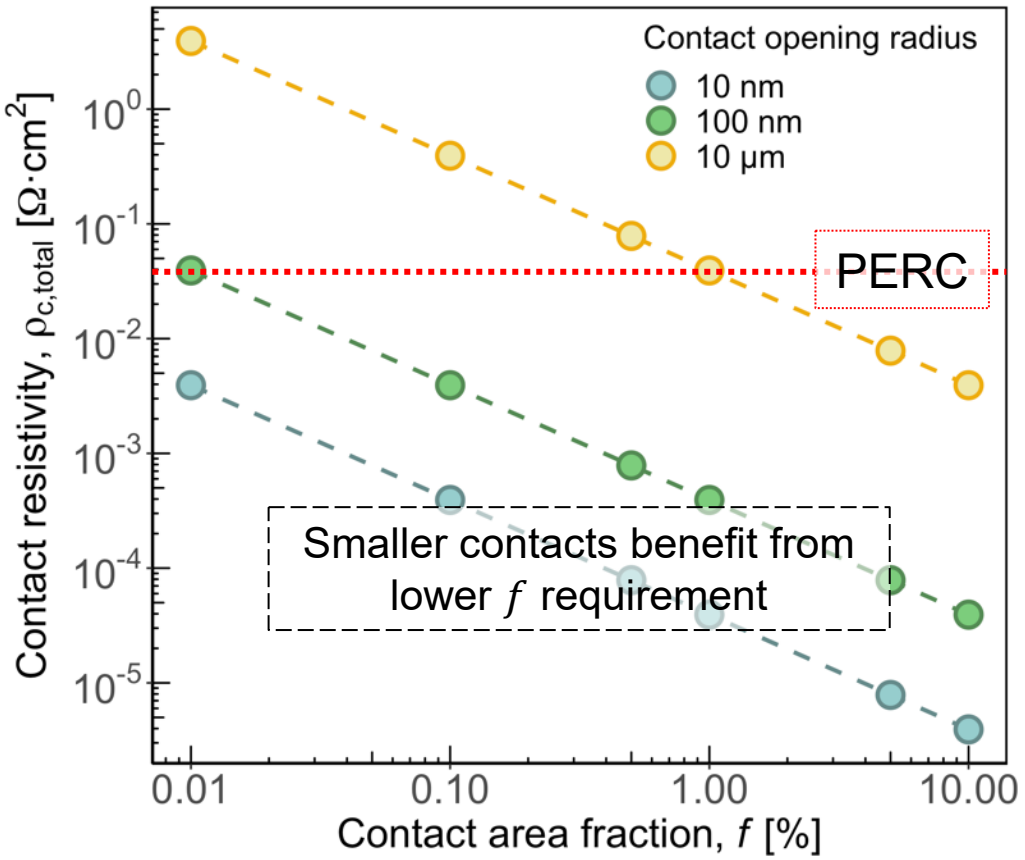

$$J_{0,total} = f \times J_{0,contact} + (1 - f) \times J_{0,passivated}$$

$$\rho_{c,total} \approx \pi \rho_w r / 4f$$

where f is the contact area fraction, ρ_w the wafer resistivity, and r the contact opening radius

[1] Denhoff, "An accurate calculation of spreading resistance," Journal of Physics D: Applied Physics. 2006.

Contact area fraction: from micron to nanoscale

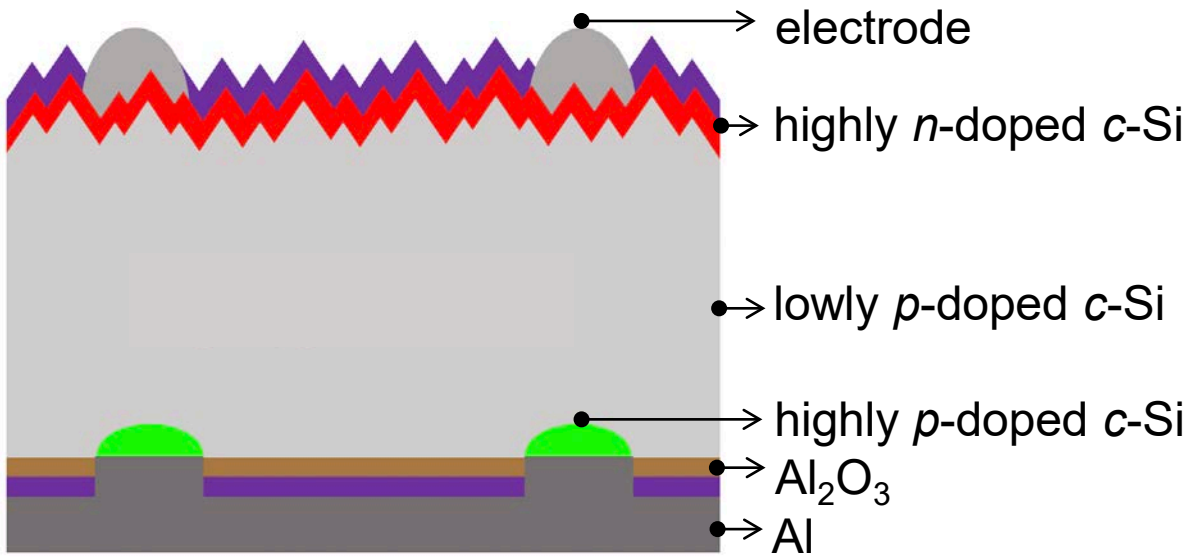

Passivated emitter and rear contact cell (PERC)

Efficiency ≈ 24% [1]

PERC limitations

- Fabrication relies on laser ablation of the rear dielectrics to form local contact openings
- Contact opening constrained to ~20–30 μm micron-wide contact openings [2]

[1] Min et al. "A roadmap towards 24% efficient PERC solar cells in industrial mass production," IEEE Journal of Photovoltaics. 2017.

[2] Dullweber and Schmidt. "Industrial silicon solar cells applying the passivated emitter and rear cell (PERC) concept – A review," IEEE Journal of Photovoltaics. 2016.

Contact area fraction: from micron to nanoscale

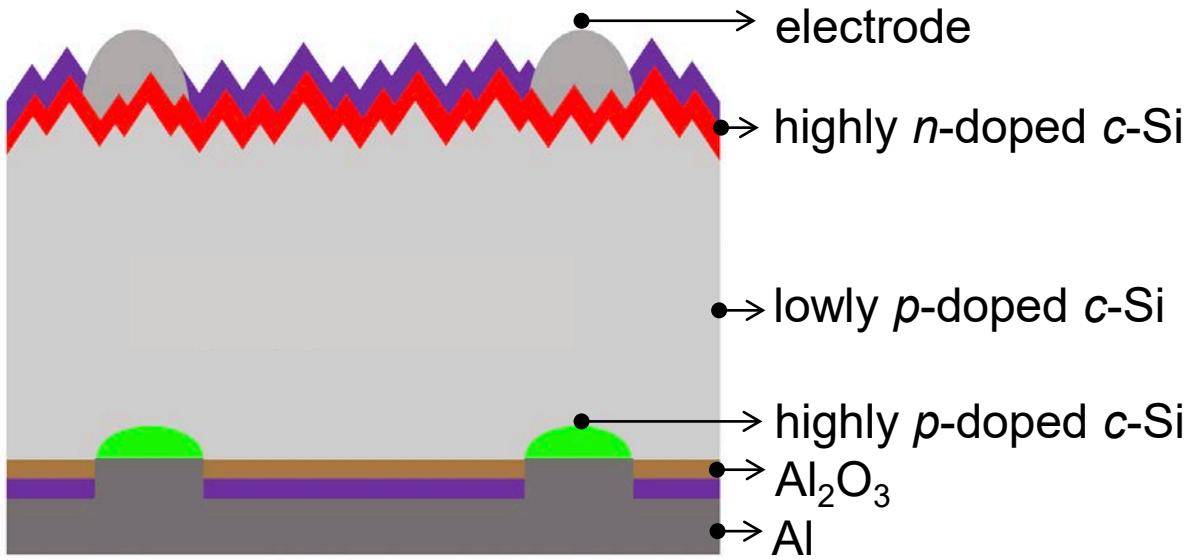

Passivated emitter and rear contact cell (PERC)

Practical efficiency $\approx 24\%$

PERC limitations

- Fabrication relies on laser ablation of the rear dielectrics to form local contact openings
- Contact opening constrained to micron-wide line contact openings

POLO contacts

- SiO_x layer provides surface passivation
- Highly-doped poly-Si confers charge-carrier selectivity
- Nanopinholes in SiO_x form at >1000°C thermal process

Polycrystalline silicon on silicon oxide (POLO)

Practical efficiency $> 25\%$

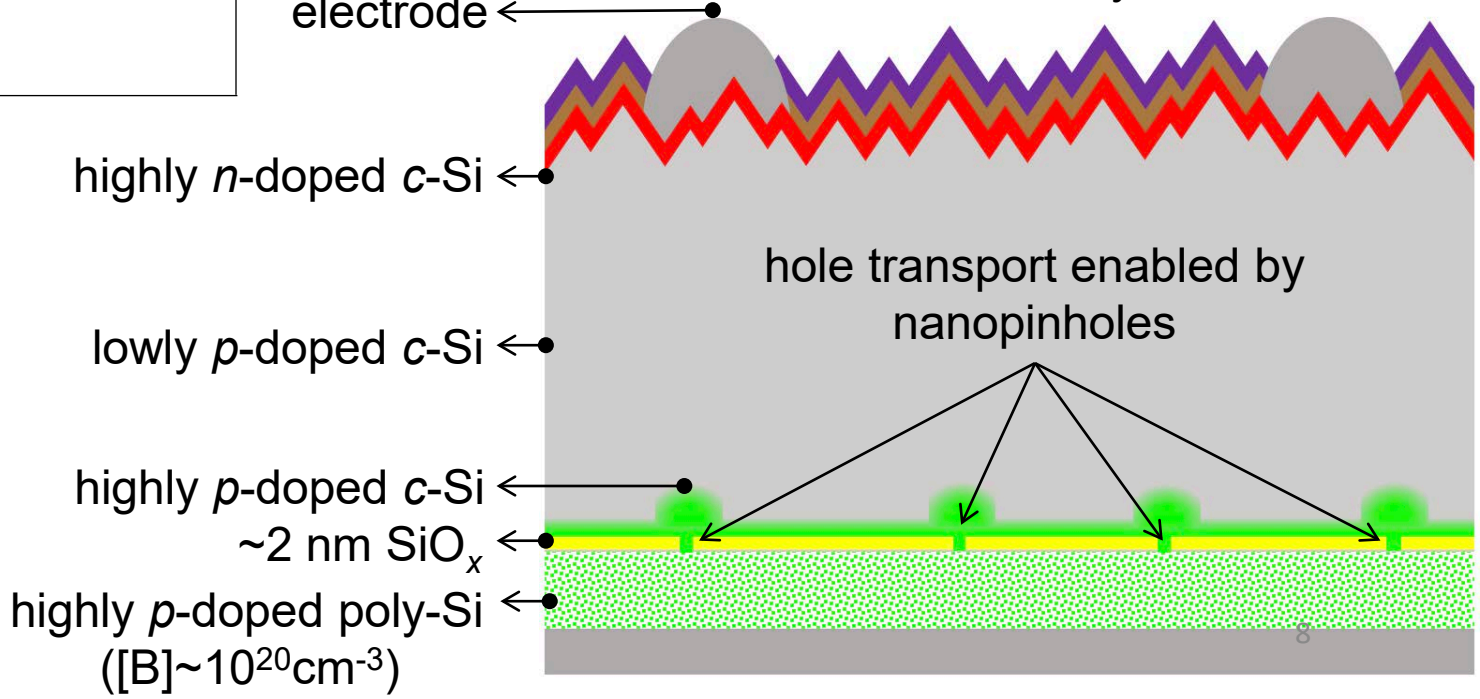

Poly-Si on locally etched dielectrics passivating contacts

- Room temperature pinhole formation
- Compatible with texture
- Compatible with passivating schemes other than ultrathin SiO_x

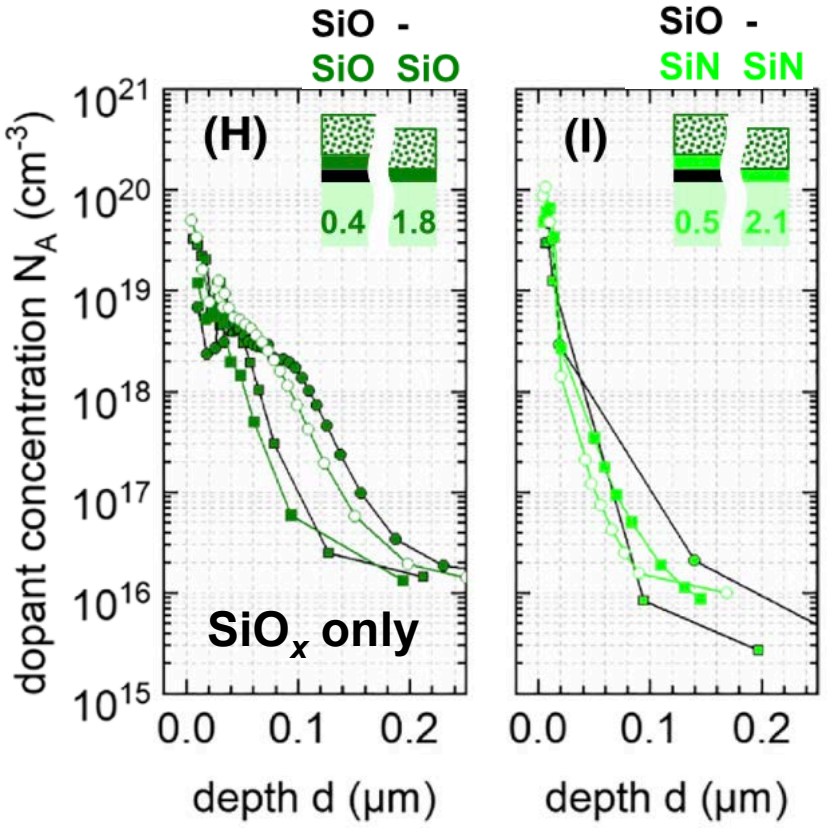

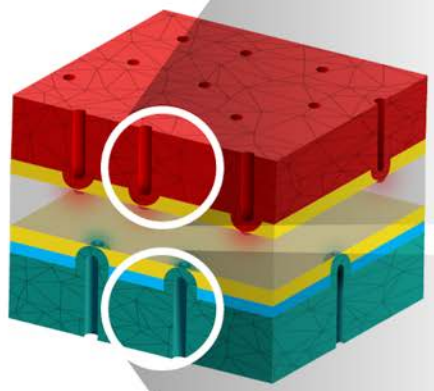

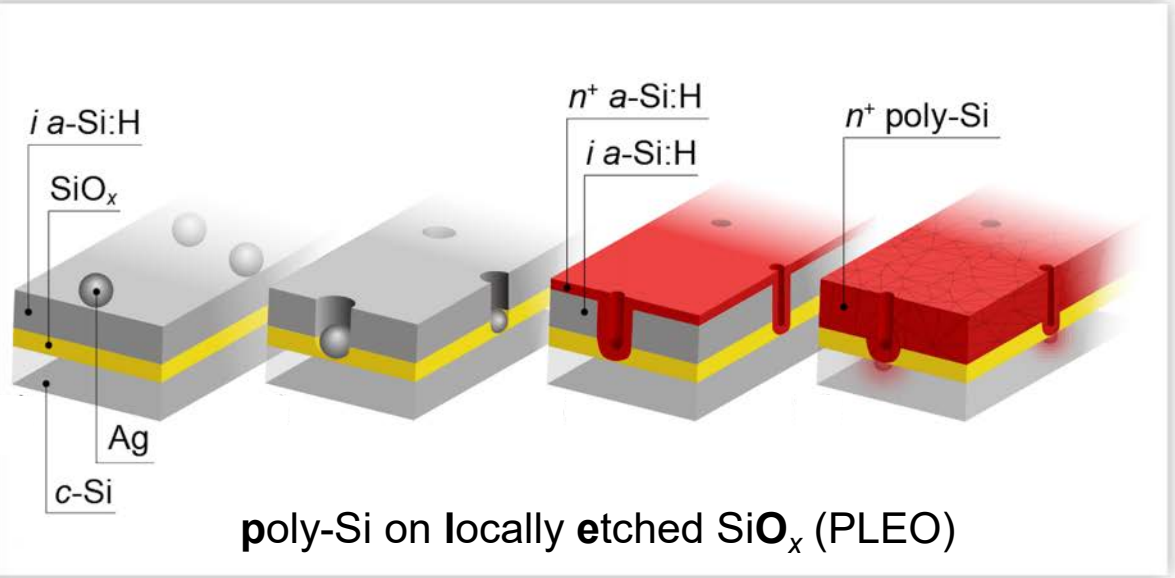

poly-Si on **l**ocally **e**tched Si**O**$_x$ (PLEO)

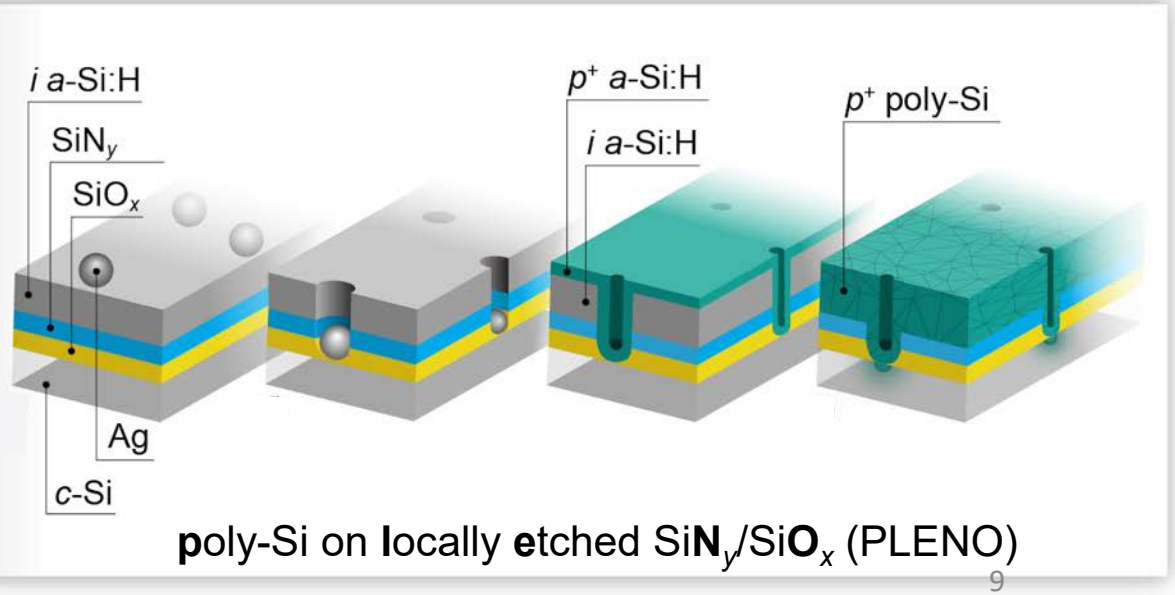

poly-Si on **l**ocally **e**tched Si**N**$_y$/Si**O**$_x$ (PLENO)

[1] Reichel et al. "Polysilicon contact structures for solar cells using atomic layer deposited oxides and nitrides as ultra-thin dielectric interlayers," Progress in Photovoltaics, 2022.

Electrons in *a*-Si:H induce the nucleation of Ag nanoparticles

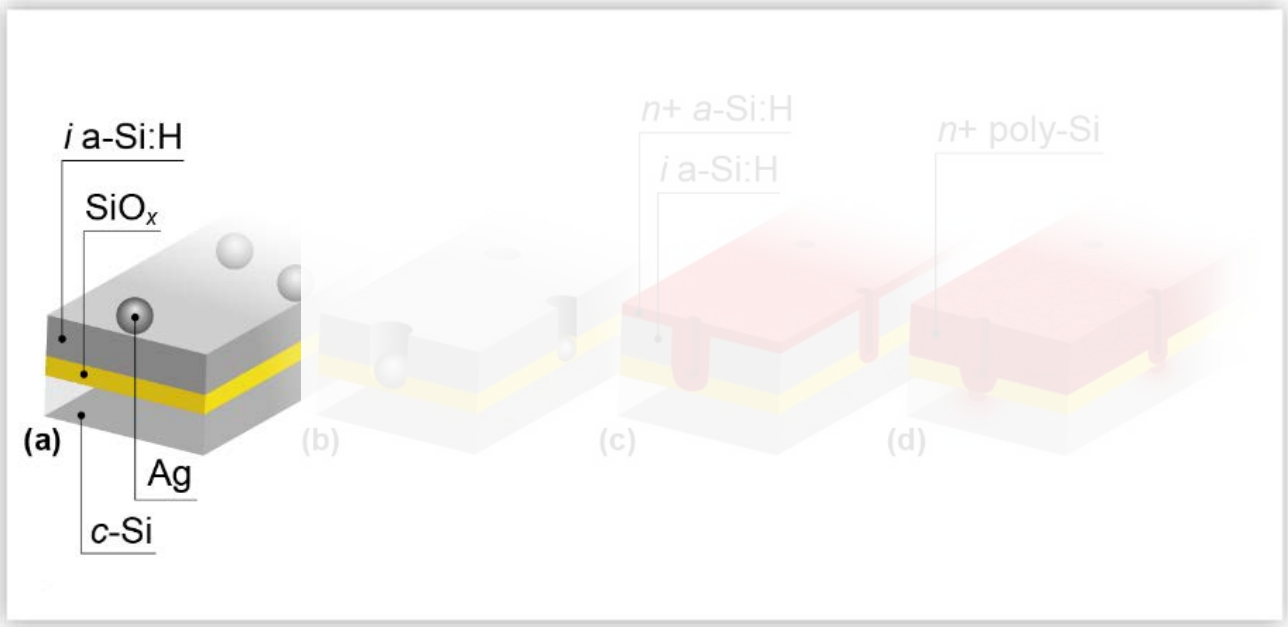

Galvanic corrosion principles are applied to locally etch pinholes

(a) Valence band electrons are supplied to Ag^+ in aqueous solution

***a*-Si in $AgNO_3$(aq)**

$$Ag^+ + e^- \rightarrow Ag^0$$

Metal-assisted chemical etching (MACE) creates mesopores in *a*-Si:H/SiO_x

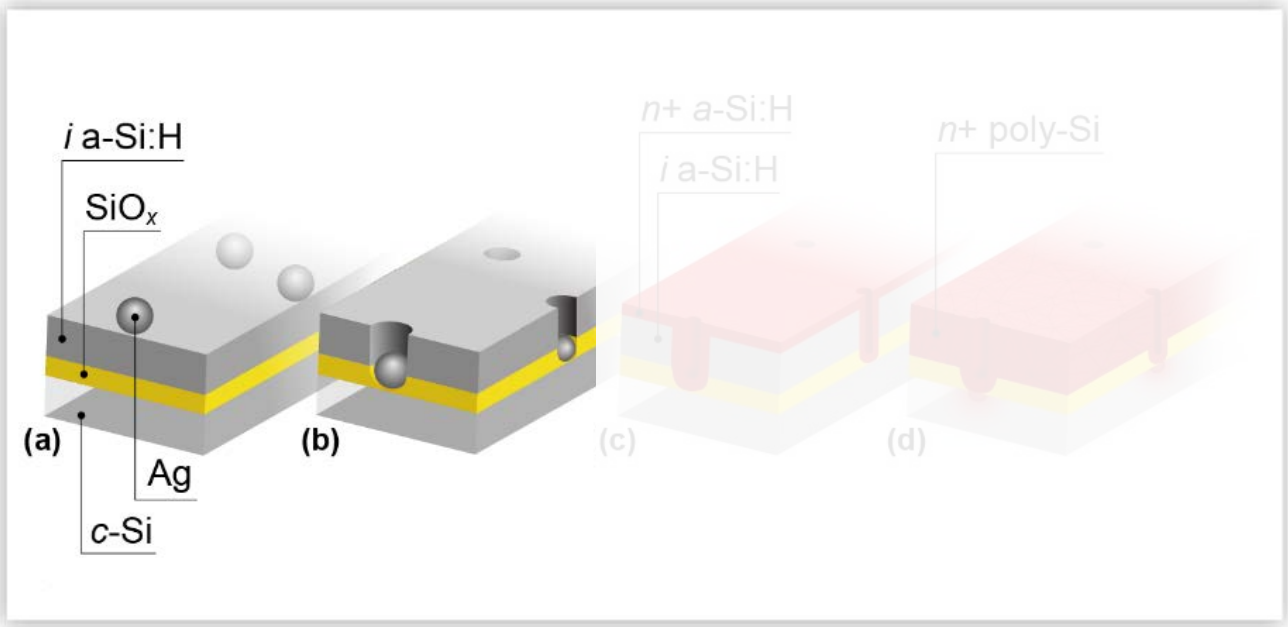

Galvanic corrosion principles are applied to locally etch pinholes

(a) Valence band electrons are supplied to Ag^+ in aqueous solution

_a_-Si in $AgNO_3$(aq)

$$Ag^+ + e^- \rightarrow Ag^0$$

(b) Local galvanic corrosion result in Ag particles "sinking" onto substrate [1] Lehmann, "Electrochemistry of Silicon," Wiley. 2002.

Ag-loaded _a_-Si in HF:H_2O_2 (aq)

Cathode reaction: $H_2O_2 + 2H^+ + 2e^- \rightarrow 2H_2O$

Anode reaction: $Si + 2H^+ \rightarrow Si^{4+} + H_2 + 2e^-$

Chemical dissolution: $Si^{4+} + 6HF \rightarrow 6H^+ + SiF_6^{2-}$

TEM reveals mesopores in *a*-Si:H/SiO_x

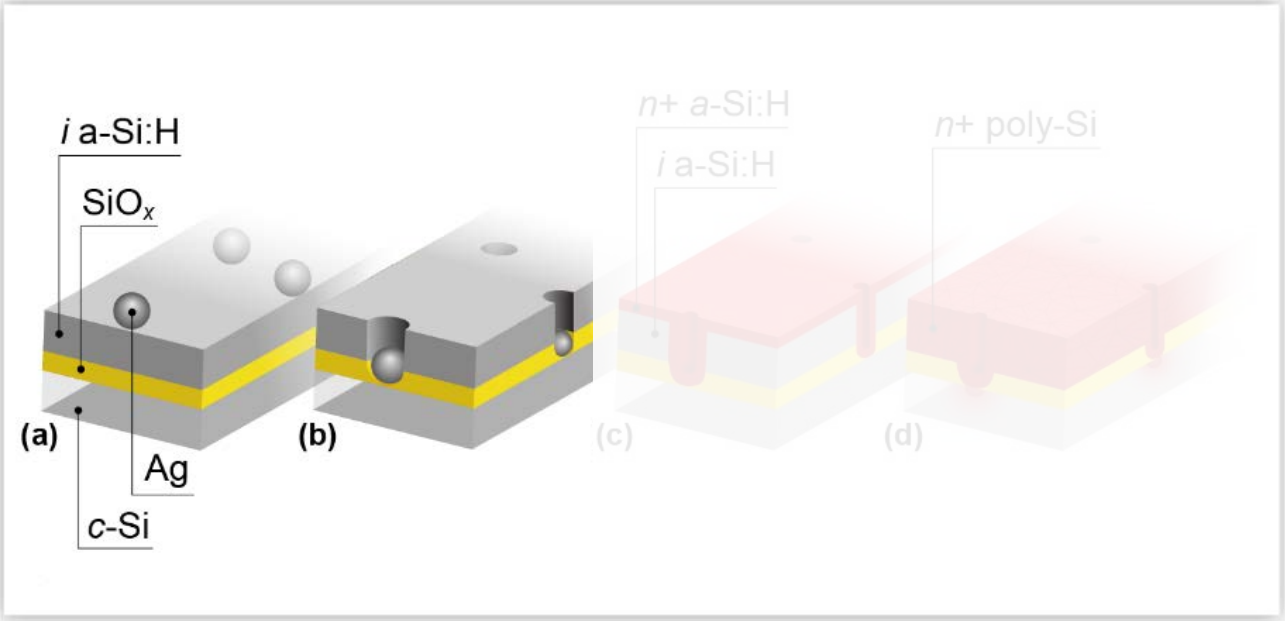

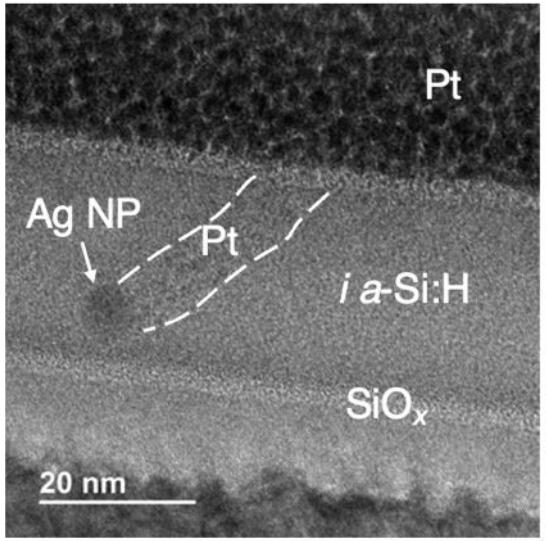

Galvanic corrosion principles are applied to locally etch pinholes

(a) Valence band electrons are supplied to Ag^+ in aqueous solution

_a_-Si in $AgNO_3$(aq)

$$Ag^+ + e^- \rightarrow Ag^0$$

(b) Local galvanic corrosion result in Ag particles "sinking" onto substrate [1] Lehmann, "Electrochemistry of Silicon," Wiley. 2002.

Ag-loaded _a_-Si in HF:H_2O_2 (aq)

Cathode reaction: $H_2O_2 + 2H^+ + 2e^- \rightarrow 2H_2O$

Anode reaction: $Si + 2H^+ \rightarrow Si^{4+} + H_2 + 2e^-$

Chemical dissolution: $Si^{4+} + 6HF \rightarrow 6H^+ + SiF_6^{2-}$

TEM reveals mesopores in *a*-Si:H/SiO_x

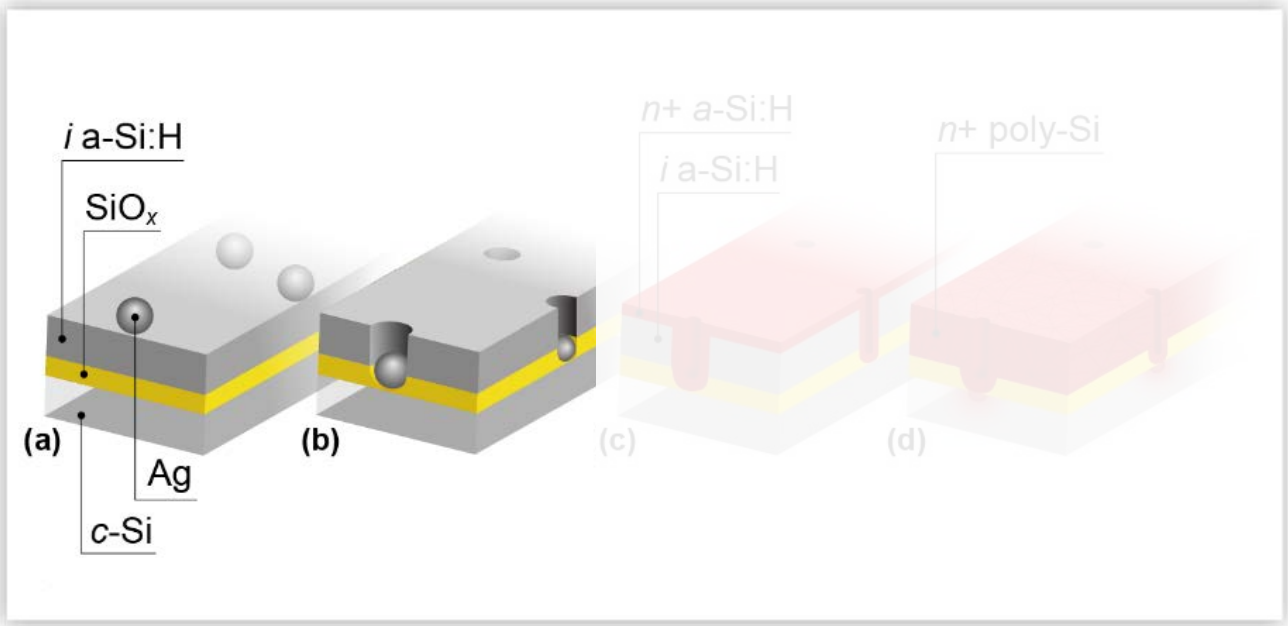

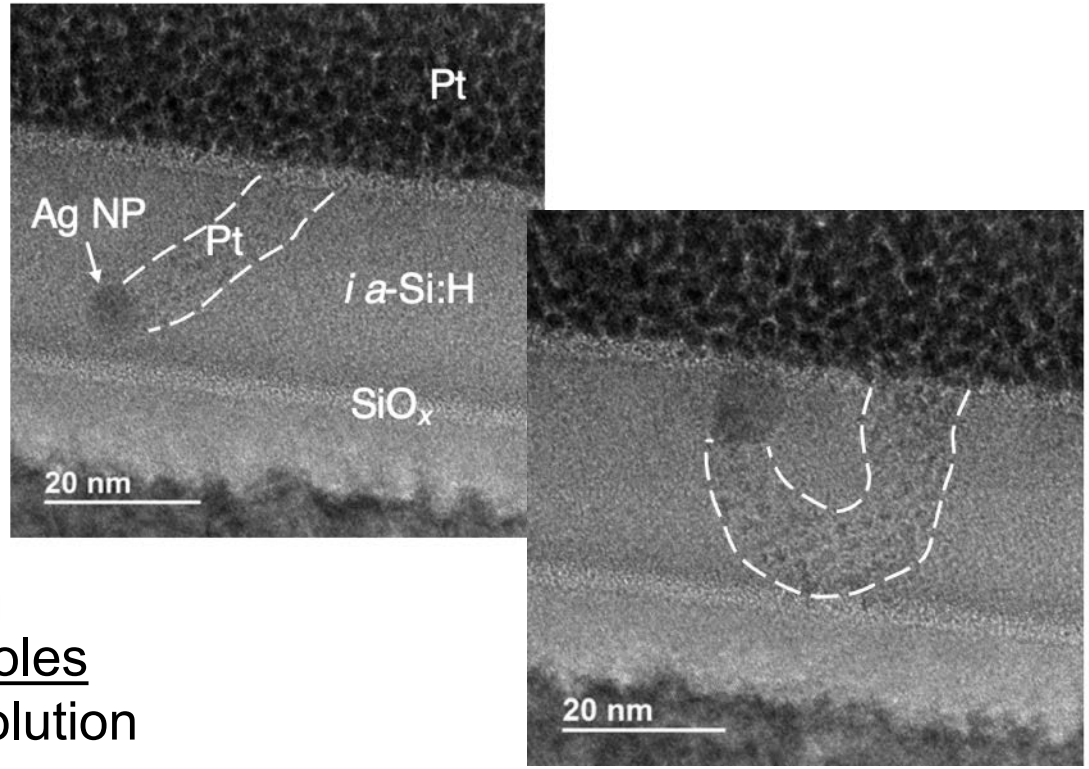

Galvanic corrosion principles are applied to locally etch pinholes

(a) Valence band electrons are supplied to Ag^+ in aqueous solution

_a_-Si in $AgNO_3$(aq)

$$Ag^+ + e^- \rightarrow Ag^0$$

(b) Local galvanic corrosion result in Ag particles "sinking" onto substrate [1] Lehmann, "Electrochemistry of Silicon," Wiley. 2002.

Ag-loaded _a_-Si in HF:H_2O_2 (aq)

Cathode reaction: $H_2O_2 + 2H^+ + 2e^- \rightarrow 2H_2O$

Anode reaction: $Si + 2H^+ \rightarrow Si^{4+} + H_2 + 2e^-$

Chemical dissolution: $Si^{4+} + 6HF \rightarrow 6H^+ + SiF_6^{2-}$

SiO_x serves as barrier to further etching of the bulk *c*-Si

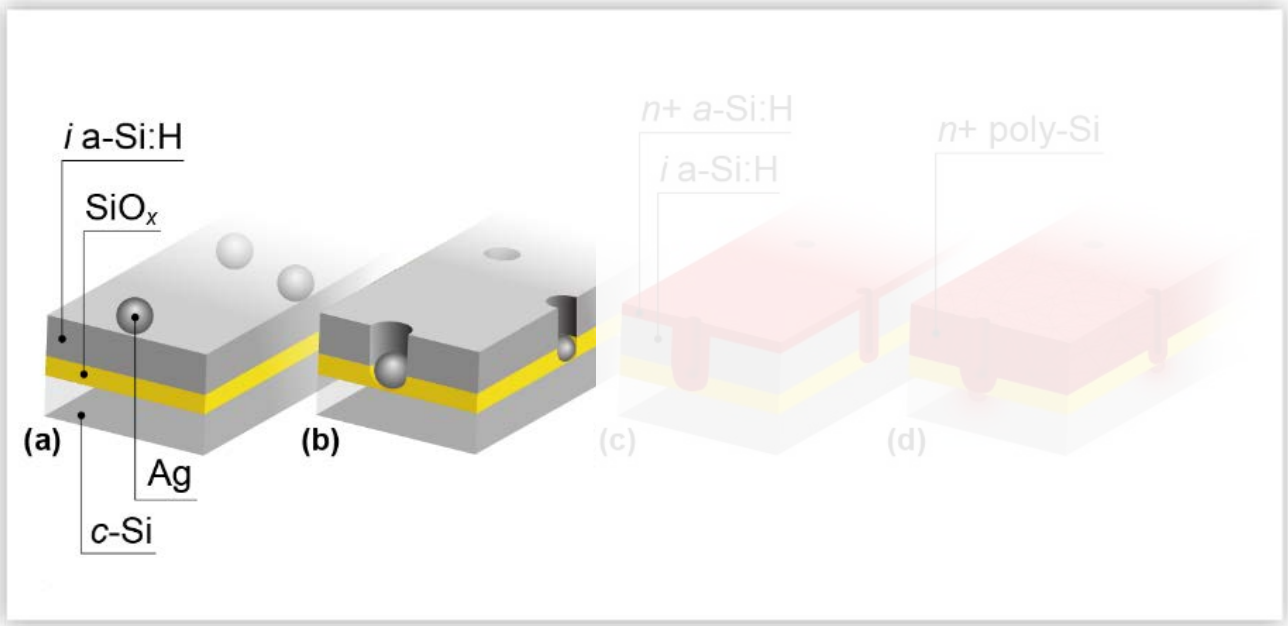

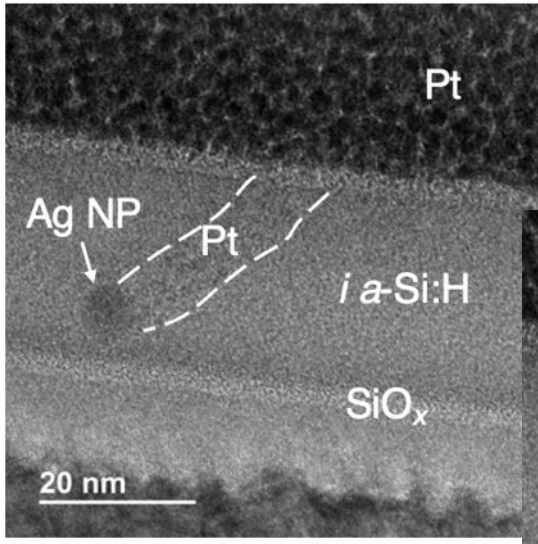

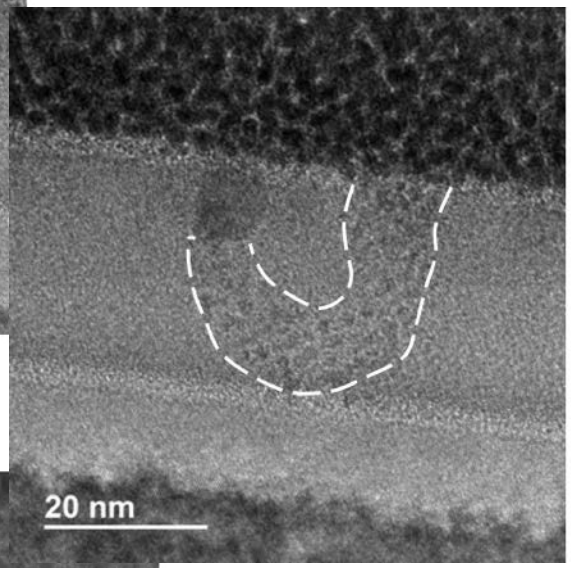

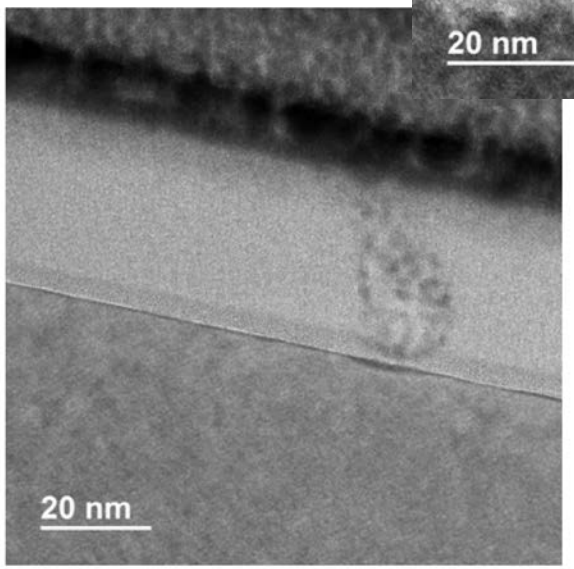

(1) Ag NP size is proportional to etching depth

(2) Not all nanoparticles create pinholes in SiO_x

(3) SiO_x serves as an effective etch “stop”

(4) SiO_x etch rate is hindered by preferential etching of *i a*-Si:H, which competitively consumes HF.

Mesopore filling turns pinholes in SiO_x accessible to electron transport

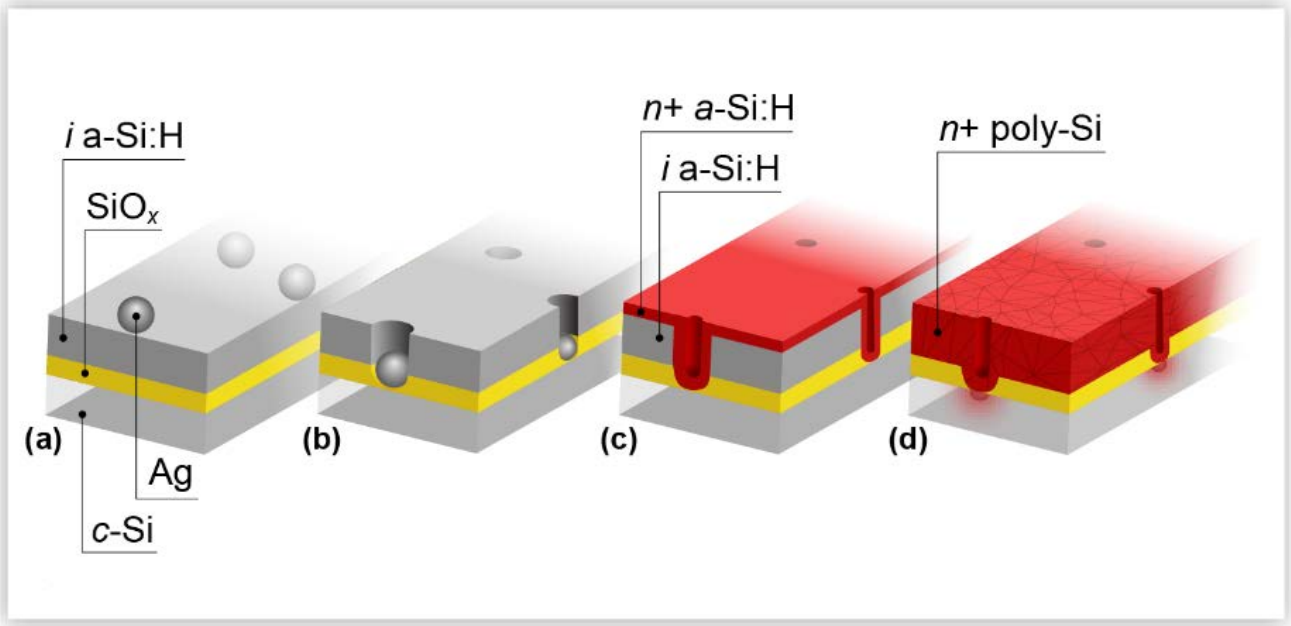

(c) PECVD of highly-doped *n*-type *a*-Si:H

(d) Thermal process for dopant drive-in and activation, and crystallization of *a*-Si:H into poly-Si; enhanced dopant diffusion at pinhole sites [1]

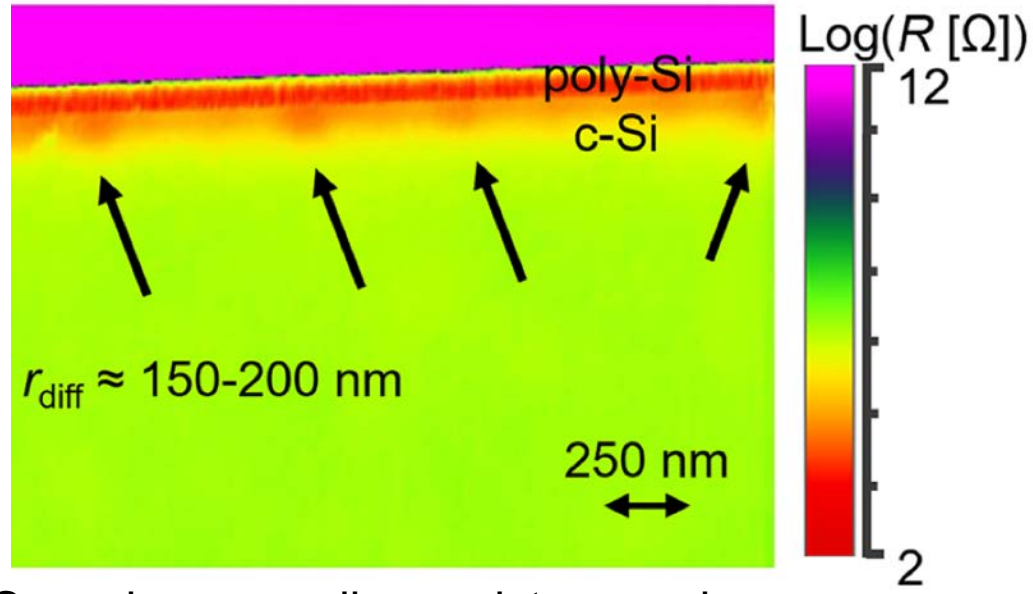

Scanning spreading resistance microscopy (SSRM)
of n^+ poly-Si/SiO_x
(thermally induced pinholes)

[1] Fırat et al., "Local Enhancement of Dopant Diffusion from Polycrystalline Silicon Passivating Contacts," ACS Applied Materials & Interfaces. 2022.

TMAH selectively etches Si over SiO_x, resulting in mesopore "magnification"

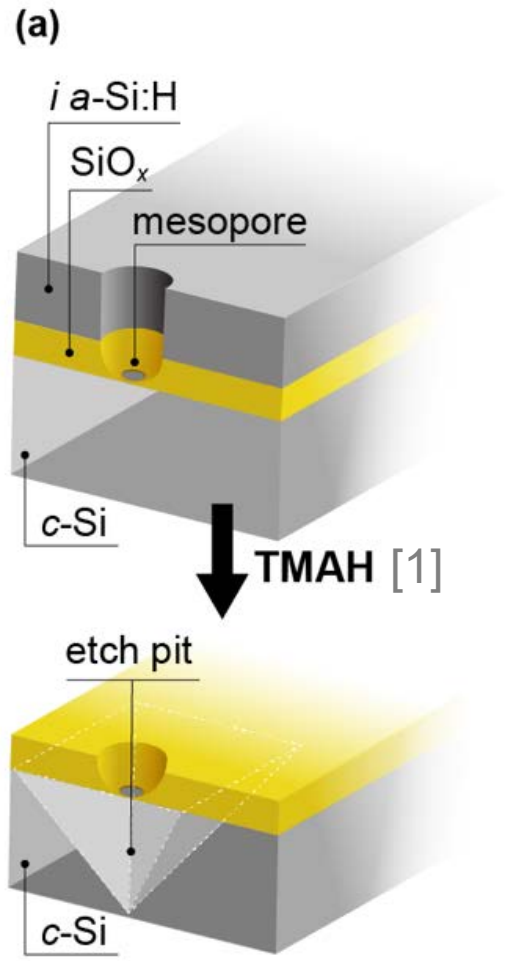

[1] Tetzlaff, "A simple method for pinhole detection in carrier selective POLO-junctions for high efficiency silicon solar cells," Solar Energy Materials and Solar Cells. 2017.

“Magnified” mesopores (i.e. etch pits) can be easily imaged

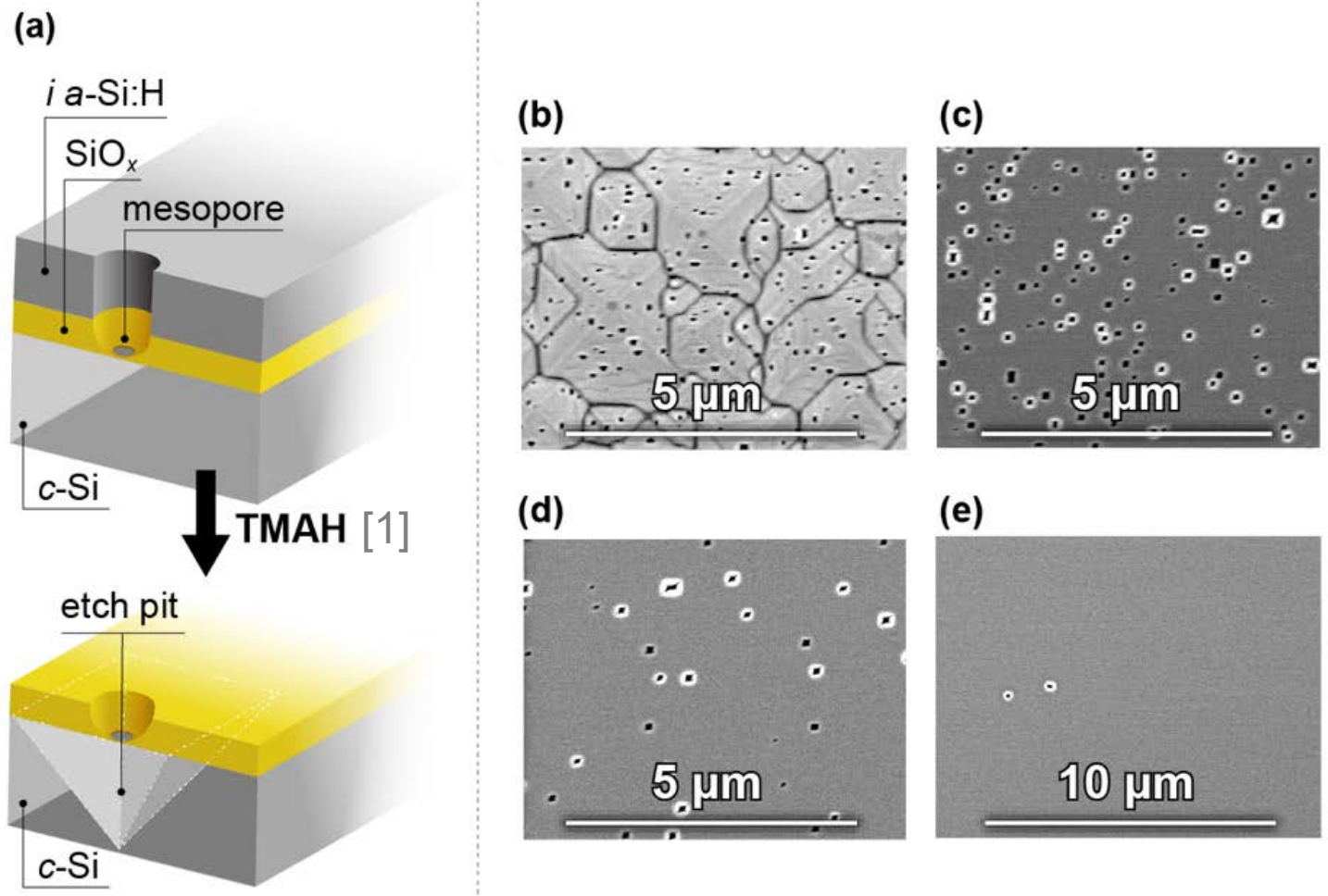

[1] Tetzlaff, “A simple method for pinhole detection in carrier selective POLO-junctions for high efficiency silicon solar cells,” Solar Energy Materials and Solar Cells. 2017.

Etching solution ($HF:H_2O_2:H_2O$) strength can be tuned to control pinhole density

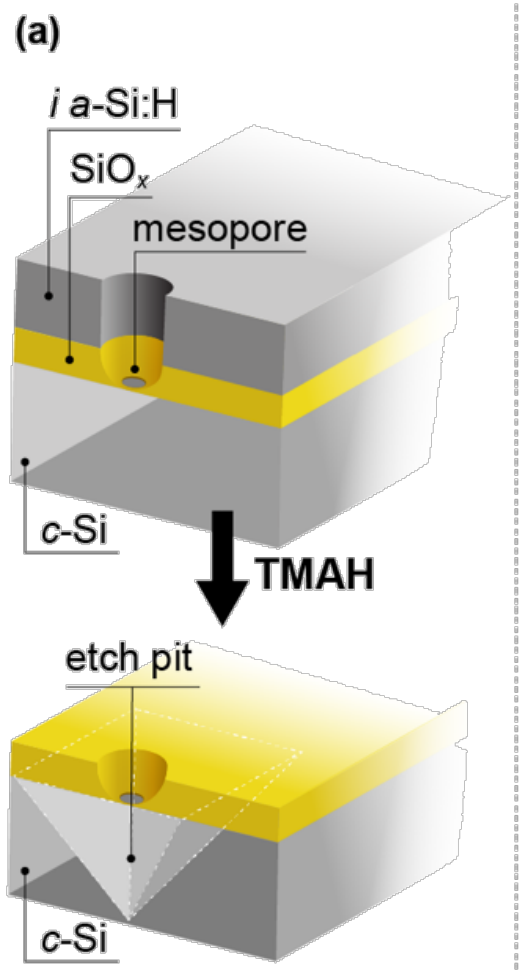

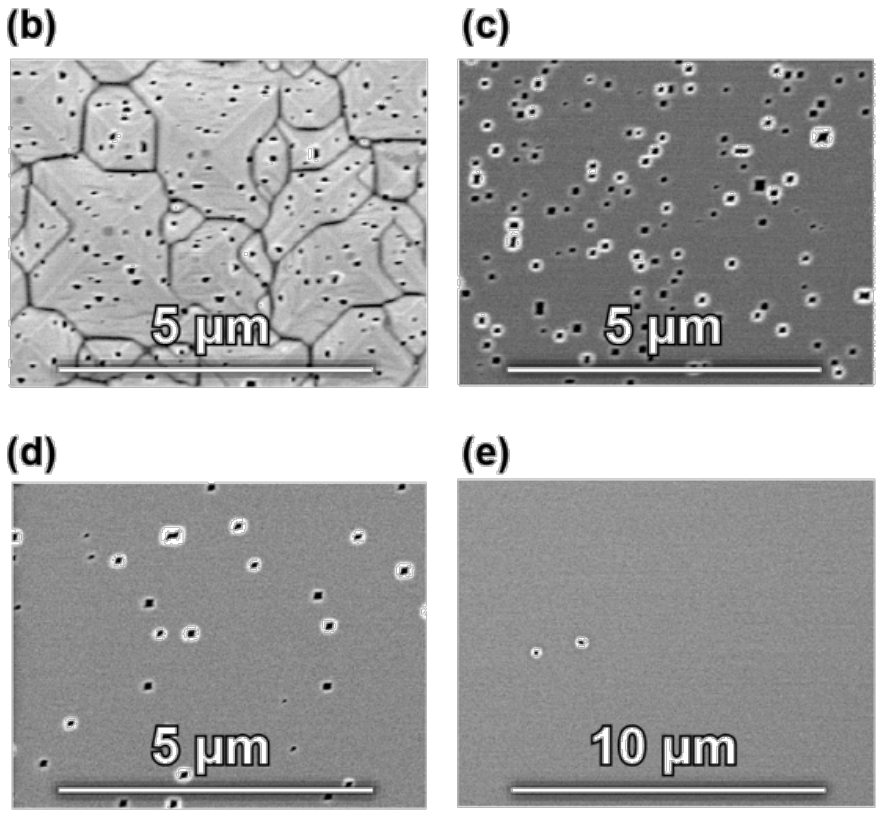

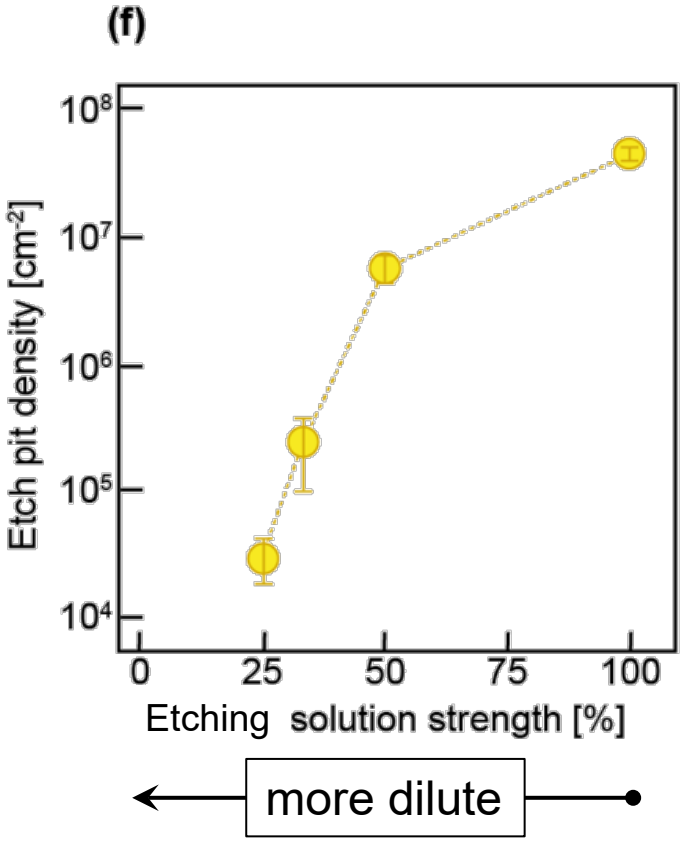

100% strength: ~ 4:3 mol/L $HF:H_2O_2$

Pinhole area density can be tuned over the range of ~10^4 to 10^8 cm^{-2}

Use of symmetric contact structures to assess passivation

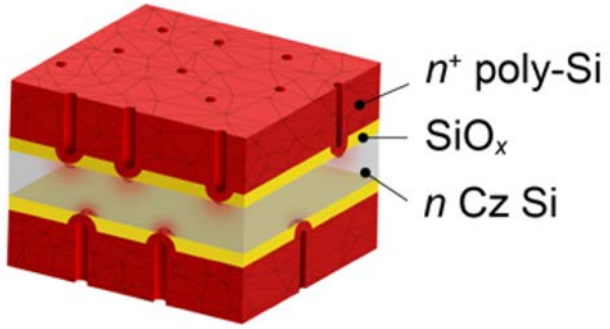

n^+ PLEO symmetric structure

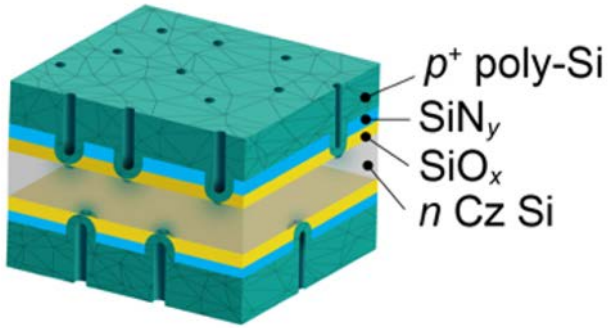

p^+ PLENO symmetric structure

iV_{OC} and J_0 for surface passivation assessment

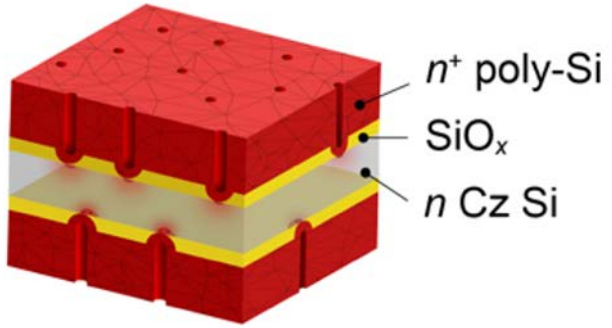

n^+ PLEO symmetric structure

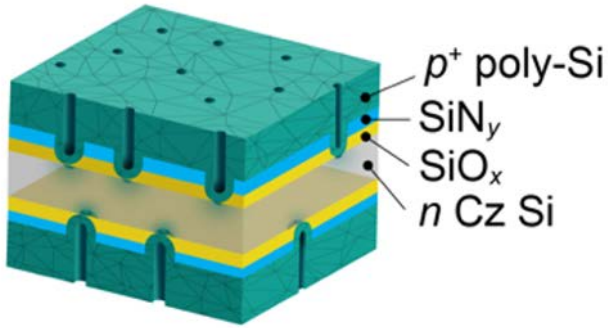

p^+ PLENO symmetric structure

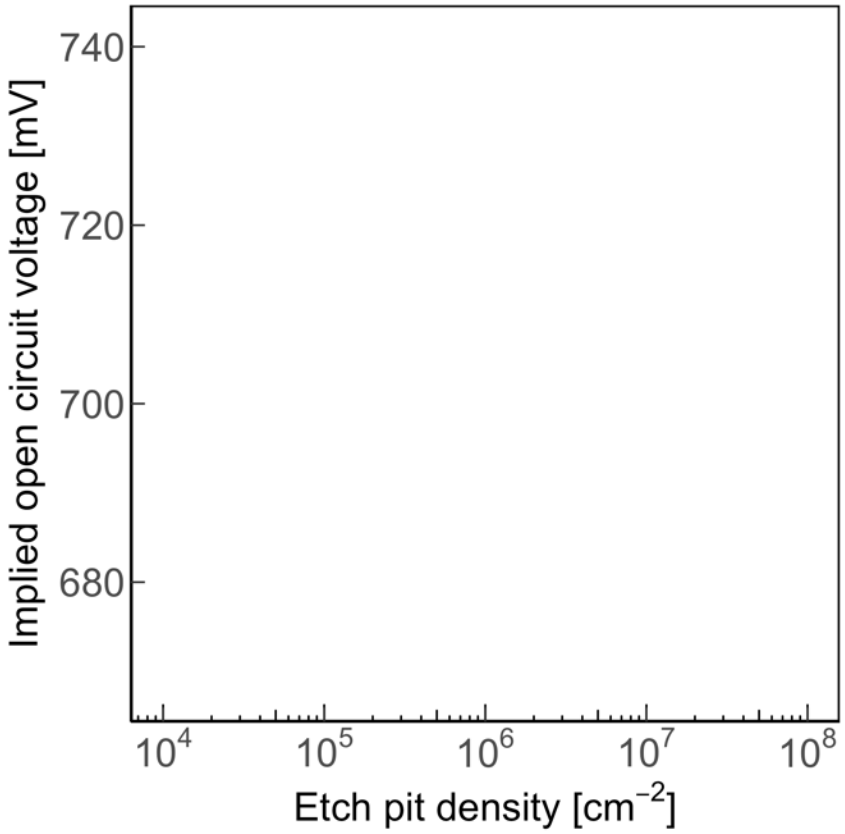

The implied open circuit voltage, iV_{OC}, is commonly used to characterize surface passivation

<u>Reminder</u>
It is desirable to maximize the iV_{OC} and minimize the J_0

n^+ PLEO on planarized *c*-Si wafers

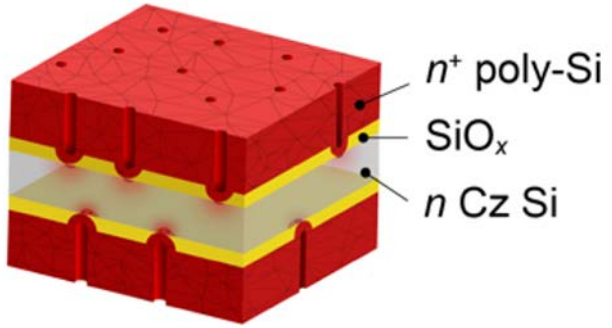

n^+ PLEO symmetric structure

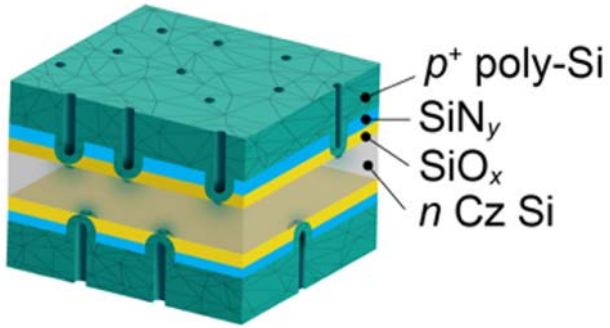

p^+ PLENO symmetric structure

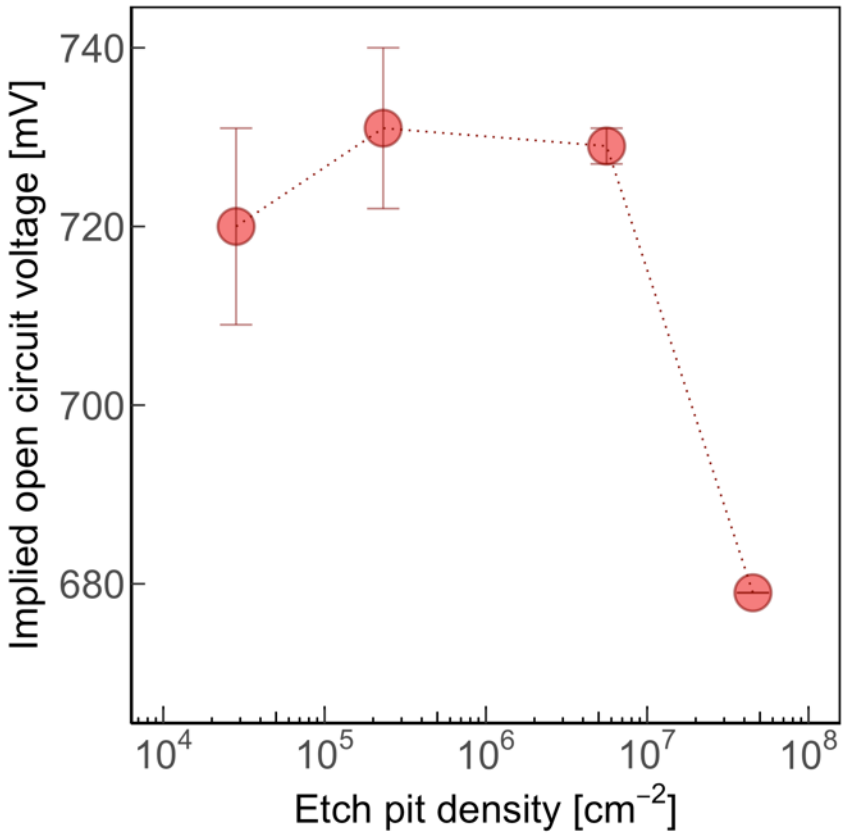

- In n^+ PLEO, iV_{OC} mostly stable until pinhole density > 10^7 cm^{-2}

Legends ◯ = planarized Si

Red = n^+ PLEO

<u>Reminder</u>
It is desirable to maximize the iV_{OC} and minimize the J_0

n^+ PLEO outperforms p^+ PLEO

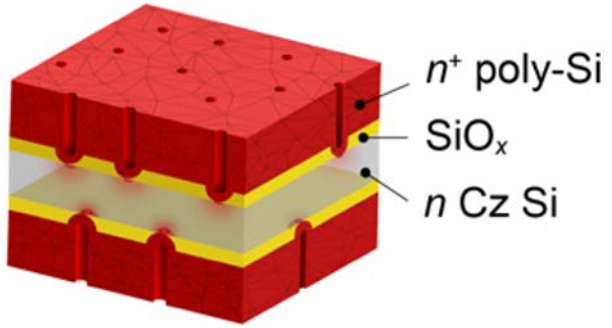

n^+ PLEO symmetric structure

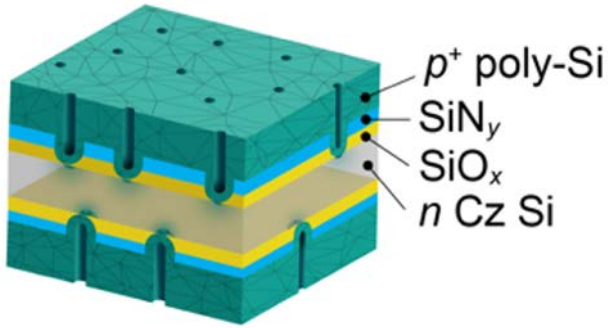

p^+ PLENO symmetric structure

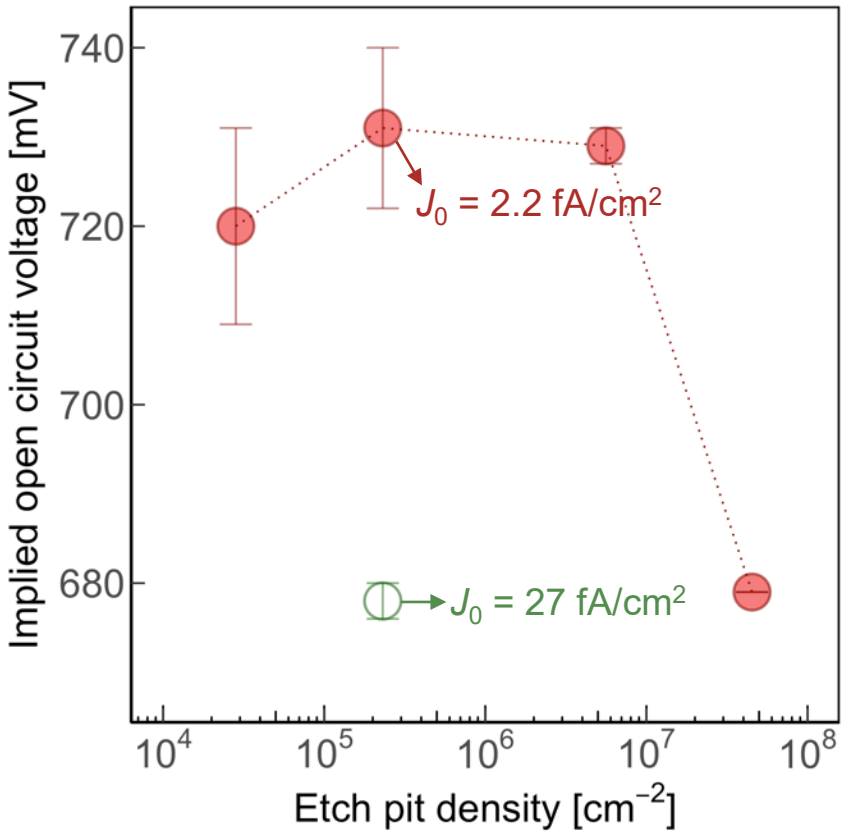

- In n^+ PLEO, iV_{OC} mostly stable until pinhole density > 10^7 cm^{-2}
- In p^+ PLEO, boron accumulation at the SiO_x [1] results in poor passivation

Legends ◯ = planarized Si

Red = n^+ PLEO

Open green = p^+ PLEO

Reminder

It is desirable to maximize the iV_{OC} and minimize the J_0

[1] Inoue et al. "Dopant distribution in gate electrode of n- and p-type metal-oxide-semiconductor field effect transistor by laser-assisted atom probe," Applied Physics Letters, 2009.

p^+ PLENO outperforms p^+ PLEO

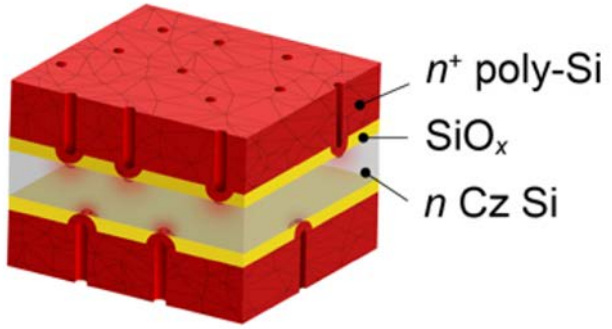

n^+ PLEO symmetric structure

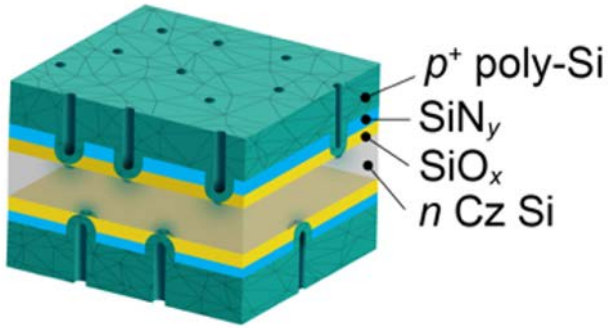

p^+ PLENO symmetric structure

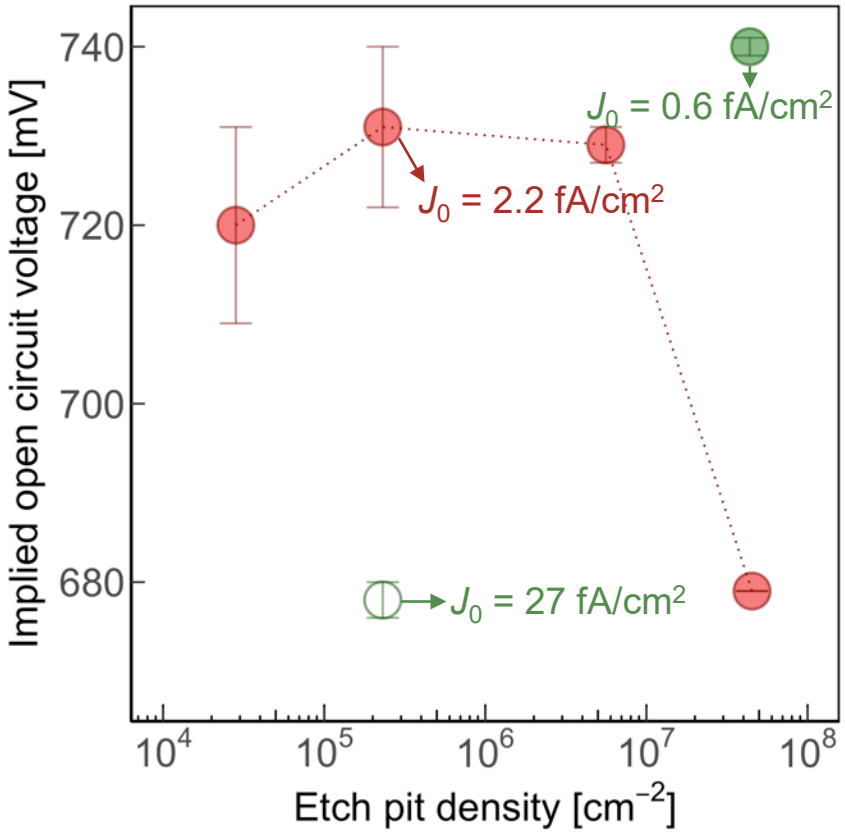

- In n^+ PLEO, iV_{OC} mostly stable until pinhole density > 10^7 cm^{-2}
- In p^+ PLEO, boron accumulation at the SiO_x [1] results in poor passivation
- SiN_y serves as dopant diffusion barrier [2]

Legends ◯ = planarized Si

Red = n^+ PLEO

Open green = p^+ PLEO

Filled green = p^+ PLENO

Reminder

It is desirable to maximize the iV_{OC} and minimize the J_0

[1] Inoue et al. "Dopant distribution in gate electrode of n- and p-type metal-oxide-semiconductor field effect transistor by laser-assisted atom probe," Applied Physics Letters, 2009.

[2] Yan et al. Passivating contacts for silicon solar cells based on boron-diffused recrystallized amorphous silicon and thin dielectric interlayers. "Solar Energy Materials and Solar Cells," 2016.

J_0 for p^+ *and* n^+ PLEO on texture is 2–3*x* higher than planarized counterparts

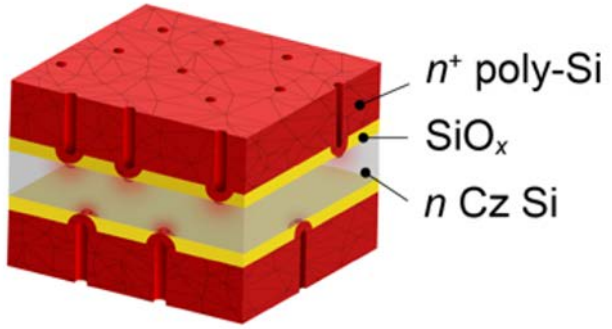

n^+ PLEO symmetric structure

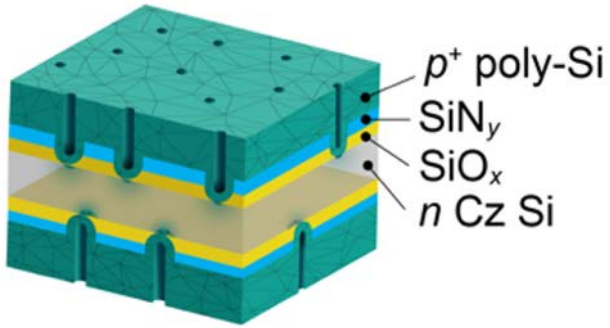

p^+ PLENO symmetric structure

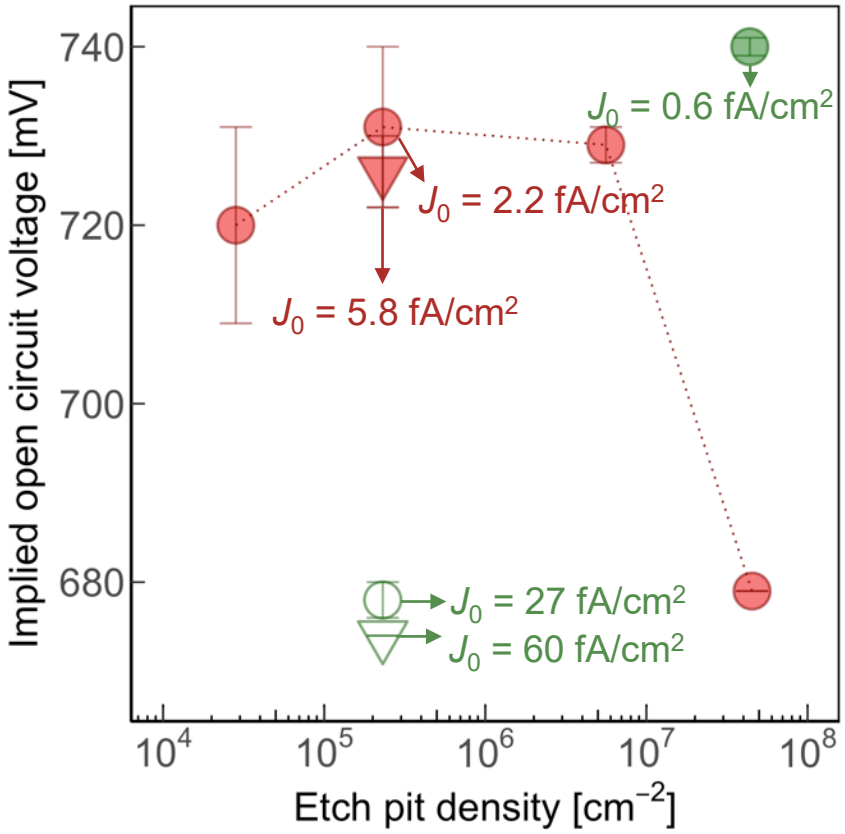

Legends

▽ = textured Si

◯ = planarized Si

Red = n^+ PLEO

Open green = p^+ PLEO

Filled green = p^+ PLENO

- In n^+ PLEO, iV_{OC} mostly stable until pinhole density > 10^7 cm^{-2}
- In p^+ PLEO, boron accumulation at the SiO_x [1] results in poor passivation
- SiN_y serves as dopant diffusion barrier [2]

Reminder

It is desirable to maximize the iV_{OC} and minimize the J_0

[1] Inoue et al. "Dopant distribution in gate electrode of n- and p-type metal-oxide-semiconductor field effect transistor by laser-assisted atom probe," Applied Physics Letters, 2009.

[2] Yan et al. Passivating contacts for silicon solar cells based on boron-diffused recrystallized amorphous silicon and thin dielectric interlayers. "Solar Energy Materials and Solar Cells," 2016.

J_0 for p^+ PLENO on texture is 7*x* higher than planarized counterpart

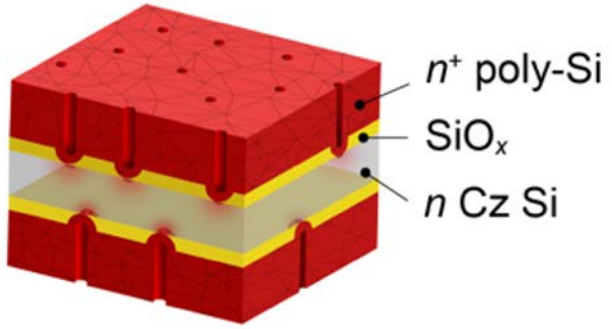

n^+ PLEO symmetric structure

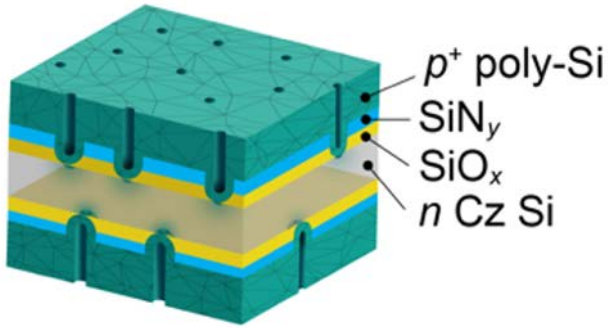

p^+ PLENO symmetric structure

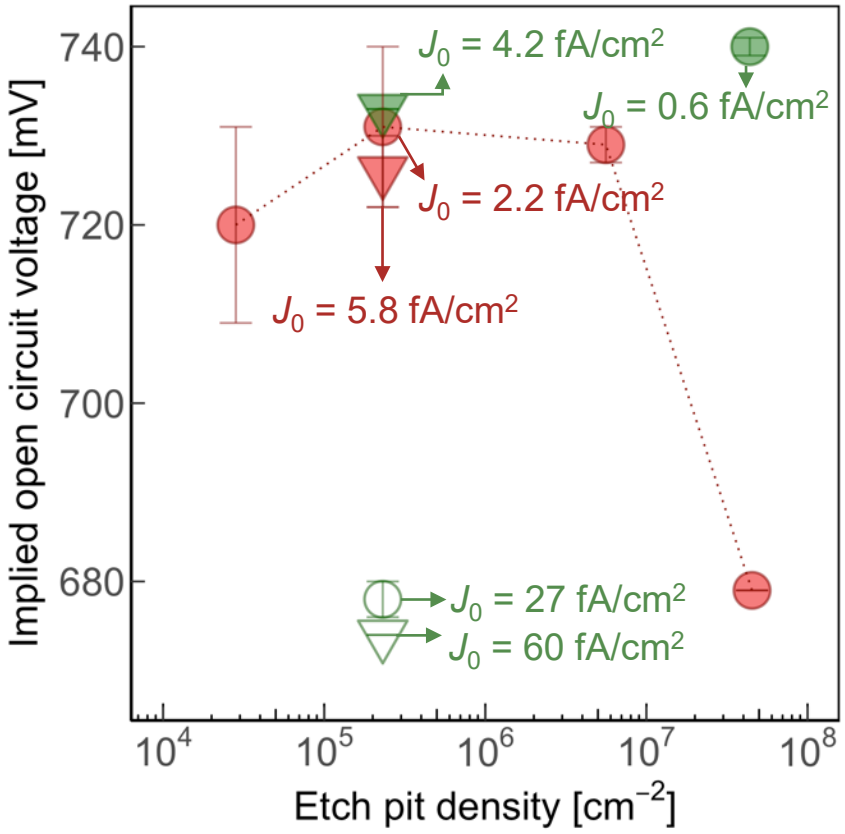

Legends

▽ = textured Si

◯ = planarized Si

Red = n^+ PLEO

Open green = p^+ PLEO

Filled green = p^+ PLENO

- In n^+ PLEO, iV_{OC} mostly stable until pinhole density > 10^7 cm^{-2}
- In p^+ PLEO, boron accumulation at the SiO_x [1] results in poor passivation
- SiN_y serves as dopant diffusion barrier [2]

Reminder

It is desirable to maximize the iV_{OC} and minimize the J_0

[1] Inoue et al. "Dopant distribution in gate electrode of n- and p-type metal-oxide-semiconductor field effect transistor by laser-assisted atom probe," Applied Physics Letters, 2009.

[2] Yan et al. Passivating contacts for silicon solar cells based on boron-diffused recrystallized amorphous silicon and thin dielectric interlayers. "Solar Energy Materials and Solar Cells," 2016.

Contact resistivity of poly-Si on locally etched dielectrics

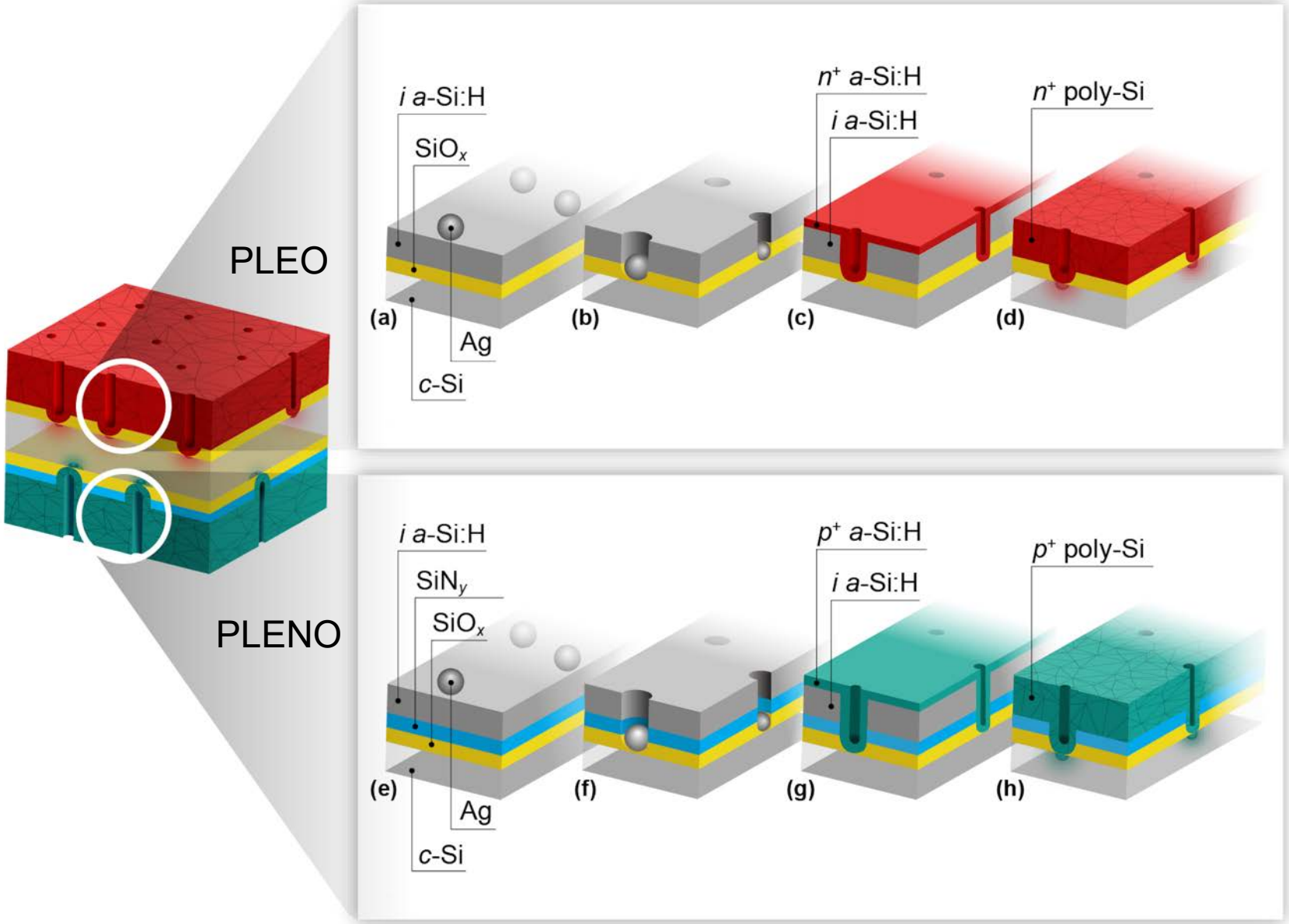

Base process for n^+ PLEO yielded well-passivated contacts with low contact resistivity, ~ 0.05 Ωcm^2

Base process for p^+ PLENO yielded well-passivated contacts with high resistivity, >1 Ωcm^2

Large etch undercut in SiN_y/SiO_x is caused by the fast etching rate of SiN_y in HF

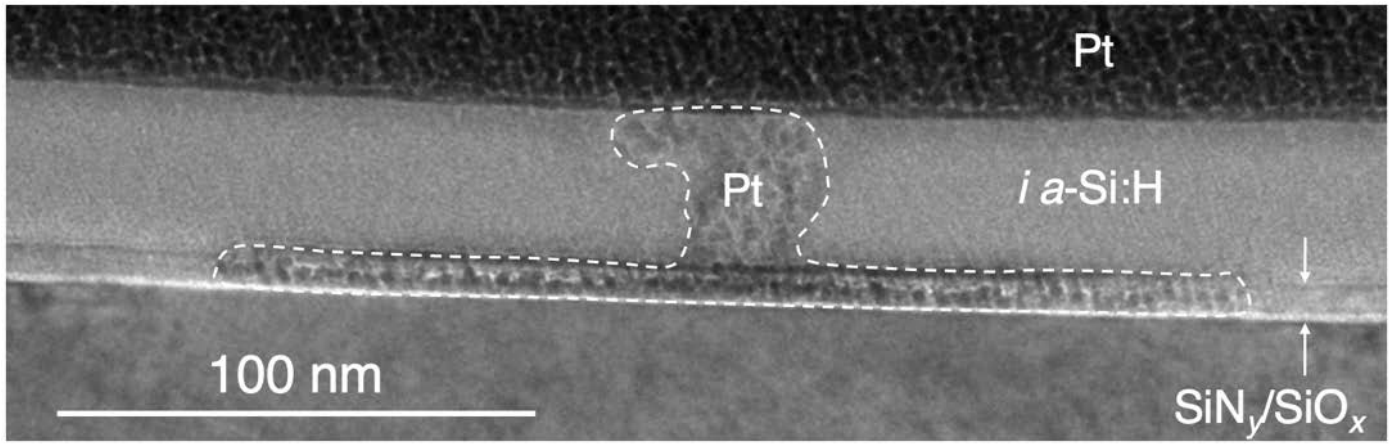

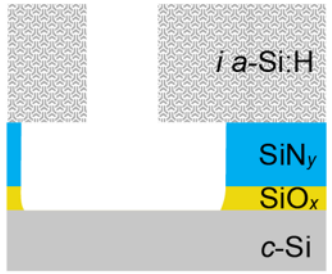

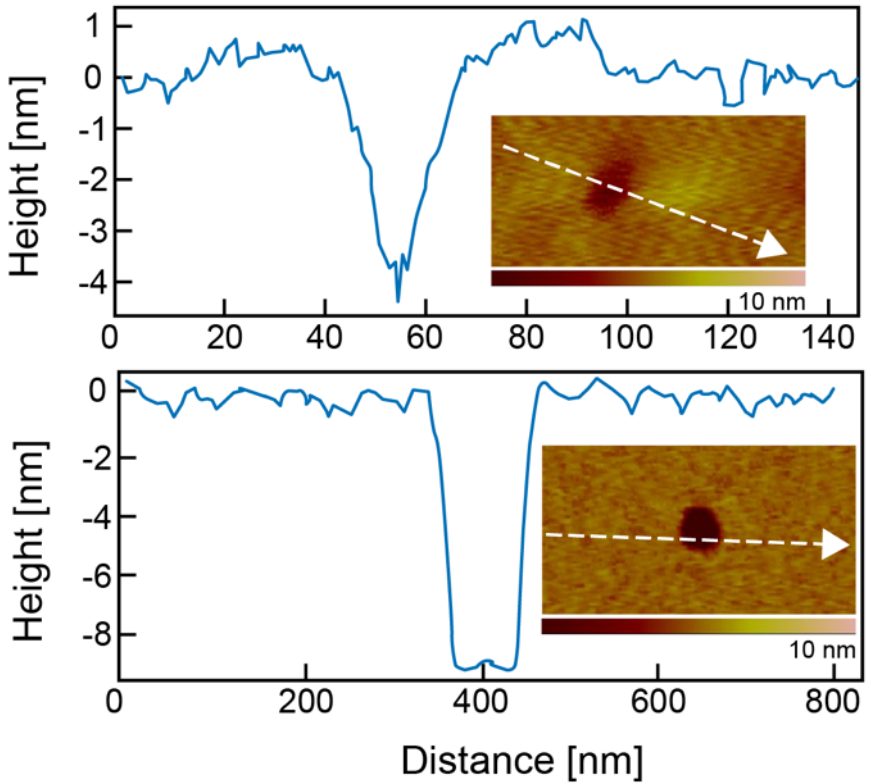

- TEM and AFM independently confirmed the existence of ~100–200 nm etch undercuts in SiN_y/SiO_x

Additional processing steps for PLENO enabled well-passivated, conducting contacts

Processing steps to mitigate SiN_y layer etch undercut

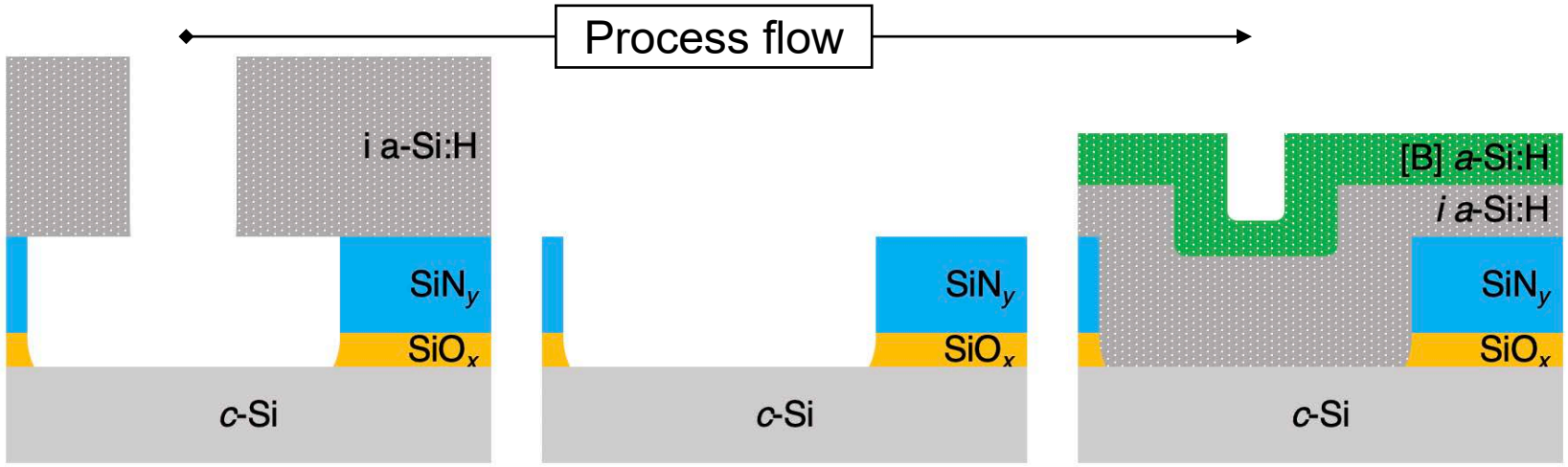

MACE-etched structure after Ag removal

Room temperature TMAH to remove *a*-Si:H

PECVD of *a*-Si:H layers

Additional processing steps ensure effective doping through SiN_y/SiO_x openings, yielding well-passivated, conducting contacts, ~0.05 Ωcm^2

Passivating contact solar cells implementing PLEO and PLENO

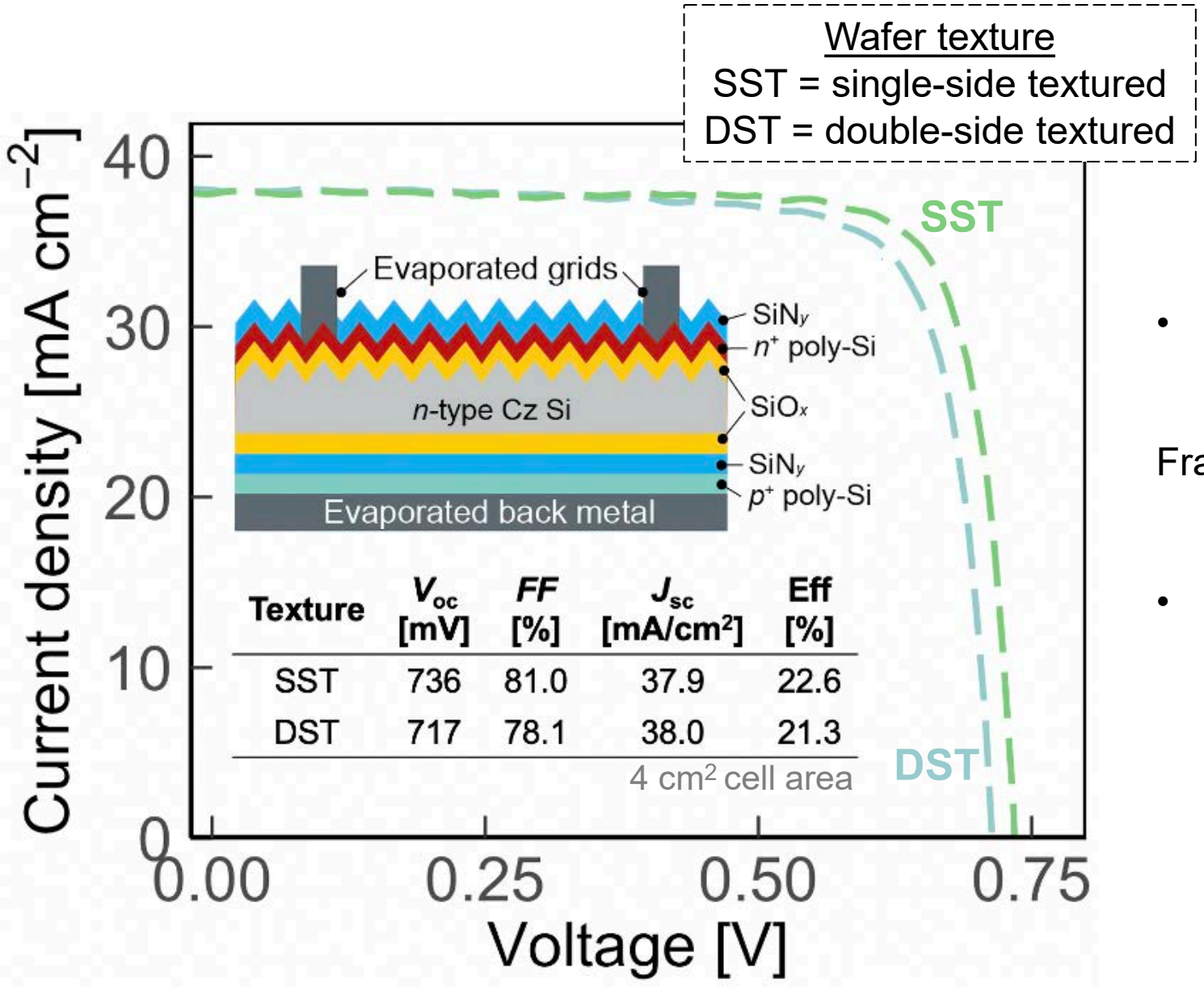

- Open-circuit voltage, V_{OC}, comparable to state-of-the-art solar cells poly-Si/SiO_x

Fraunhofer-ISE: 26.0% efficiency with 732.3 mV
ISFH: 26.1% efficiency with 726.6 mV

- Moderate short-circuit current density, J_{SC} caused by parasitic absorption at front poly-Si contact

Comparison with state-of-the-art pinhole-enabled poly-Si contacts

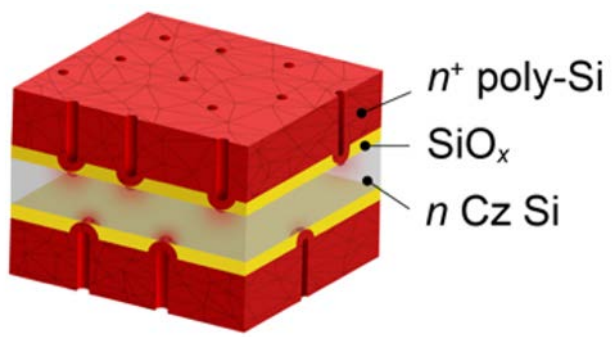

n^+ PLEO symmetric structure

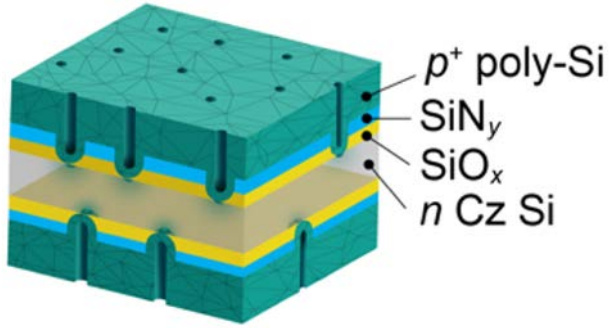

p^+ PLENO symmetric structure

Surface morphology	Recombination parameter, J_0 [fA/cm^2]			
	n^+ PLEO	n^+ POLO	p^+ PLENO	p^+ POLO
planarized	2.2	6.0[1]	0.6	5.0[1]
random pyramids	5.8	--	4.2	--

[1] Hollemann et al. "Separating the two polarities of the POLO contacts of an 26.1%-efficient IBC solar cell," Nature Scientific Reports. 2020.

- PLEO & PLENO contact resistivities still about one order of magnitude higher than POLO

Industrial relevance

- SiN_y composition needs to be tuned to prevent etch undercut
- Integrate rear PLENO with industrially-relevant cell fabrication (no poly-Si contact in the front)
- Bottom-up technoeconomic analysis still needed

SolarTech in-line MACE tool

In-line tools compatible with room temperature pinhole creation chemical processes already used by PV industry for texturing of wafers [1]

[1] Jooss et al., 33rd European Photovoltaic Solar Energy Conference and Exhibition. 2017.

Summary

- Nanoscale contact openings offer desirable tradeoffs in passivation and conductivity
- Nanogalvanic corrosion was used to fabricate nanopinhole passivating contacts
- Introducing a SiN_y layer between SiO_x and p^+-poly resulted in 45*x* lower recombination parameter J_0 due to doping being constrained to pinhole sites
- Undercut in SiN_y/SiO_x correlated to high resistance contacts; more investigations are needed
- Textured n^+ PLEO and p^+ PLENO passivation comparable to planarized n^+ and p^+ POLO
- Best proof-of-concept cell achieved 22.6% efficiency with 736 mV for open circuit voltage

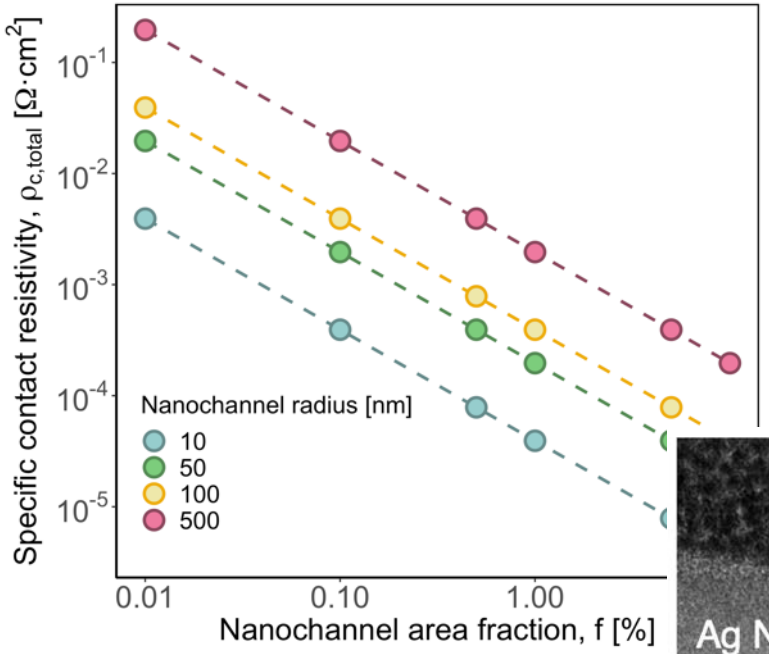

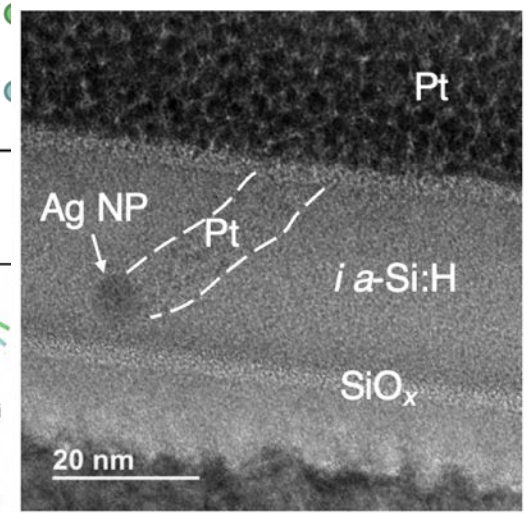

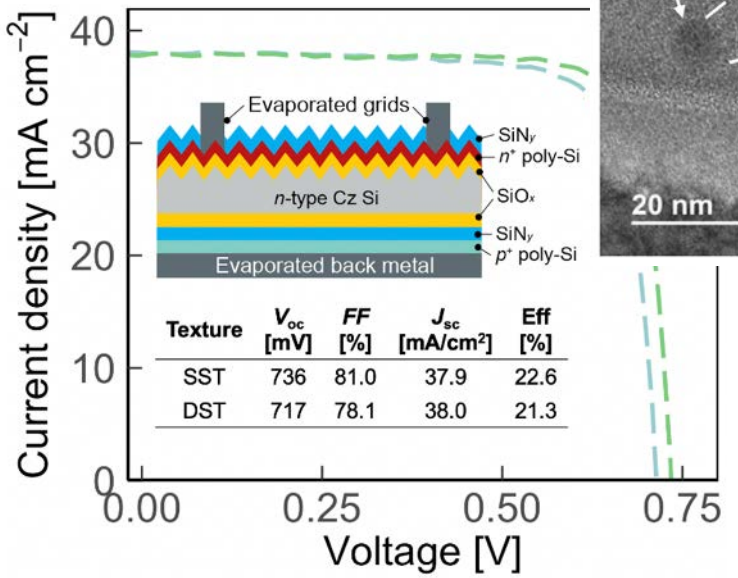

Texture	V_{oc} [mV]	*FF* [%]	J_{sc} [mA/cm²]	Eff [%]
SST	736	81.0	37.9	22.6
DST	717	78.1	38.0	21.3

Acknowledgement

Funding source U.S. Department of Energy (DOE)
under Contract No. DE-AC36-08GO28308

NREL team
Kejun Chen
Dr. Ryan France
Dr. Harvey Guthrey
Matthew (Matt) Hartenstein
Dr. Chun-Sheng (CS) Jiang
Markus Kaupa
Vincenzo (Vinnie) LaSalvia
Dr. Suchismita (Suchi) Mitra
Chirag Mule
William (Bill) Nemeth
Matthew (Matt) Page
Dirk Steyn
San Theingi
Dr. Paul Stradins (PI)
Dr. David Young

Mines group
Dr. Sumit Agarwal (PI)
Kejun Chen
Matthew Hartenstein
Andrew Kaye
Chirag Mule
Wallis Scholl
Dirk Steyn
Xue Wang

Mentors (alumni)
Dr. Abhijit Kale
Dr. Abigail Meyer


Joshua Bauer


Werner Slocum

NREL Transforming ENERGY

U.S. DEPARTMENT OF ENERGY
Energy Efficiency & Renewable Energy

COLORADOSCHOOLOFMINES
EARTH • ENERGY • ENVIRONMENT

Contact area opening at the nanoscale: fabrication methods

Mainstream protocols

The tunneling and thermal SiO_x breakup approaches

- Very sensitive to sub-nanoscale SiO_x thickness variability [1]
- So far only industrially deployed on: planarized, electron-selective contacts, with quantum-tunneling SiO_x
- If thicker SiO_x, nanopinholes must be formed under high thermal budget (> 1000 °C)

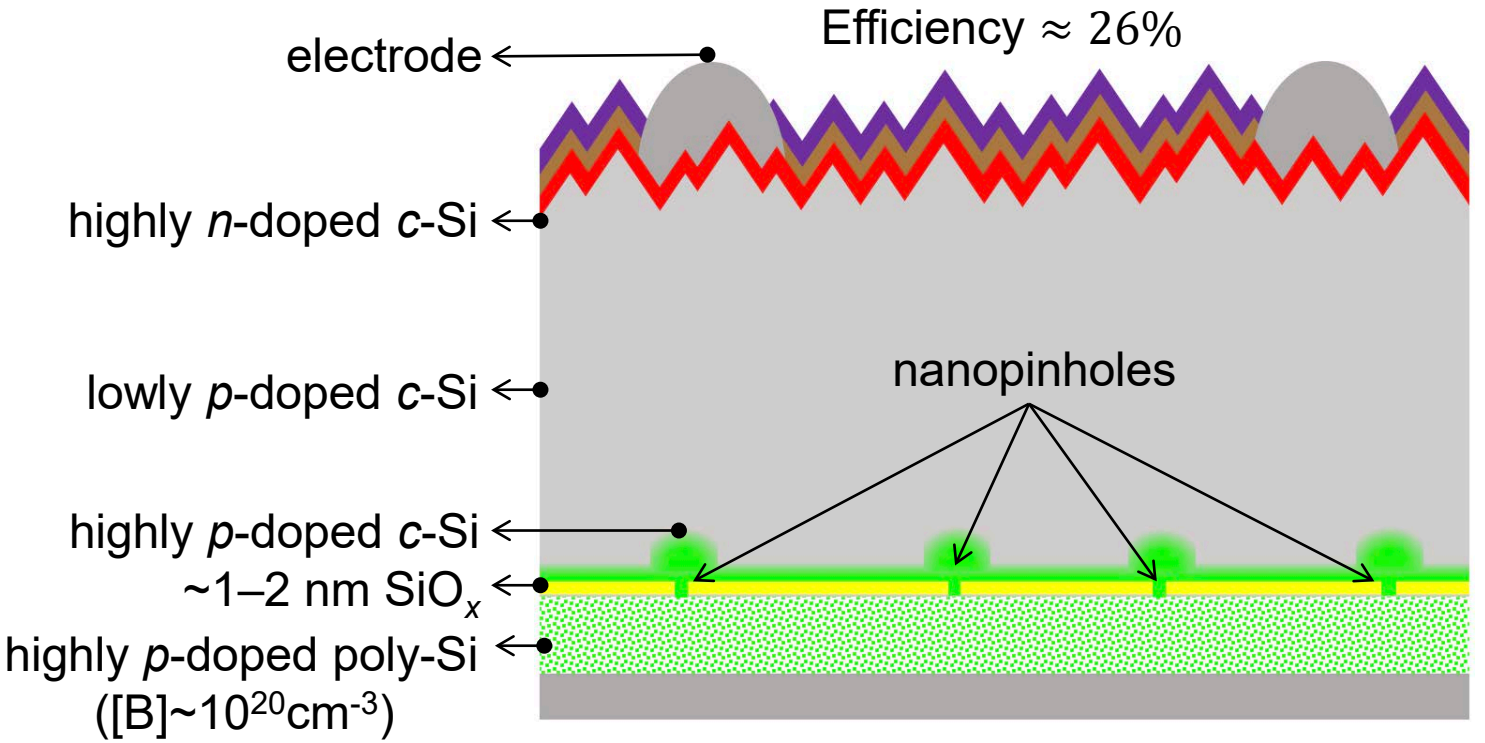

[1] Wang et al. "Influence of SiOx film thickness on electrical performance and efficiency of TOPCon solar cells," Solar Energy Materials and Solar Cells. 2020.
[2] Haase et al. "Laser contact openings for local poly-Si-metal contacts enabling 26.1%-efficient POLO-IBC solar cells," Solar Energy Materials and Solar Cells. 2018.

Our protocol

The room temperature chemical etching approach [3]

- Nanopinholes formed at room temperature, using wet chemistry
- Compatible with textured surfaces
- Not constrained to ultrathin SiO_x

[3] Lima Salles et al. "Nano-pinhole passivating contact Si solar cells fabricated with metal-assisted chemical etching," under external review.

Enhanced dopant in-diffusion at pinhole sites

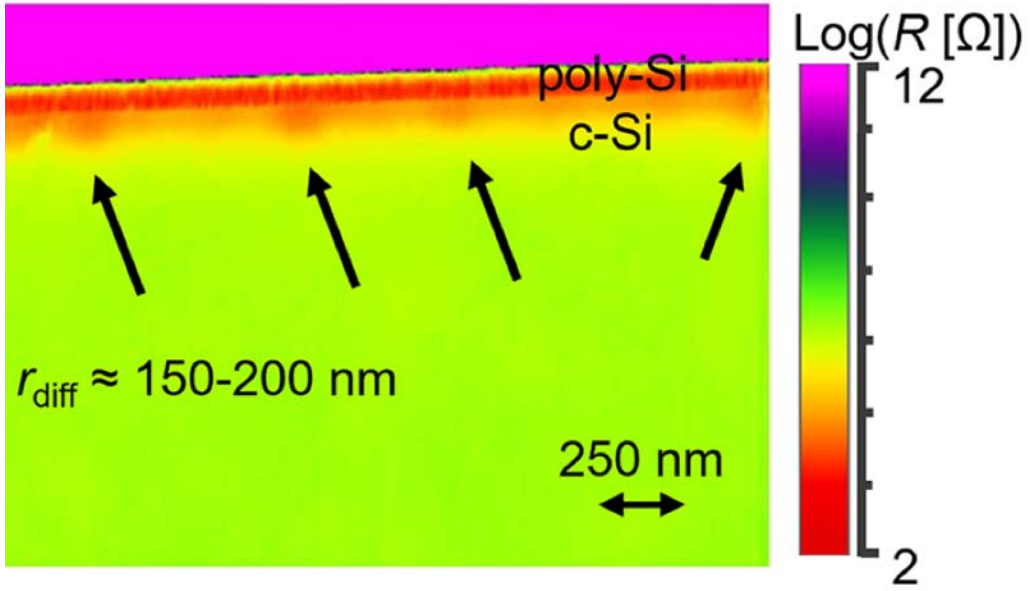

Scanning spreading resistance microscopy (SSRM) of n^+ poly-Si/SiO_x

- ~1.2 nm SiO_x
- SSRM enhanced-diffusion area density estimations: 2.8×10^8 to 4×10^8 cm^{-2}
- Area density estimations by SSRM matches pinhole density estimations closely: 4×10^8 cm^{-2}

Fırat et al., "Local Enhancement of Dopant Diffusion from Polycrystalline Silicon Passivating Contacts," ACS Applied Materials & Interfaces. 2022.

Challenges in the fabrication of poly-Si/SiO_x contacts

- Passivation and conductivity parameters are very sensitive to sub-nanoscale variations in the SiO_x thickness
- Unavoidable variability in SiO_x thickness critically reduces their yield/throughput in mass production
- p^+ poly-Si/SiO_x: boron accumulation in SiO_x constrains poly-Si contact deployment to n^+ poly-Si/SiO_x only
- Poor performance when applied to textured morphologies

<u>Less-stringent method to fabricate poly-Si contacts is in order</u>

- flexibility over choice of passivating dielectric scheme
- applicable to texture
- lower sensitivity to variations in dielectric thickness

I–V parameters of TOPCon cells.

Item		Voc	J_{sc}	R_{ser}	FF	Eff
SiO_x [nm]		(mV)	(mA/cm^2)	mΩ	(%)	(%)
1.55	Median	687.1	39.92	4.64	81.09	22.25
	Best cell	689.4	40	4.34	81.35	22.43
1.25	Median	679	39.82	6.18	78.5	21.23
	Best cell	682.2	39.91	5.97	78.71	21.43
1.43	Median	680.1	39.8	5.23	79.94	21.7
	Best cell	684	39.94	5.22	79.78	21.79

Wang, Q. et al. *Solar Energy Materials and Solar Cells*. 2020. https://doi.org/10.1016/j.solmat.2019.110258

Silicon solar cells: source of efficiency losses

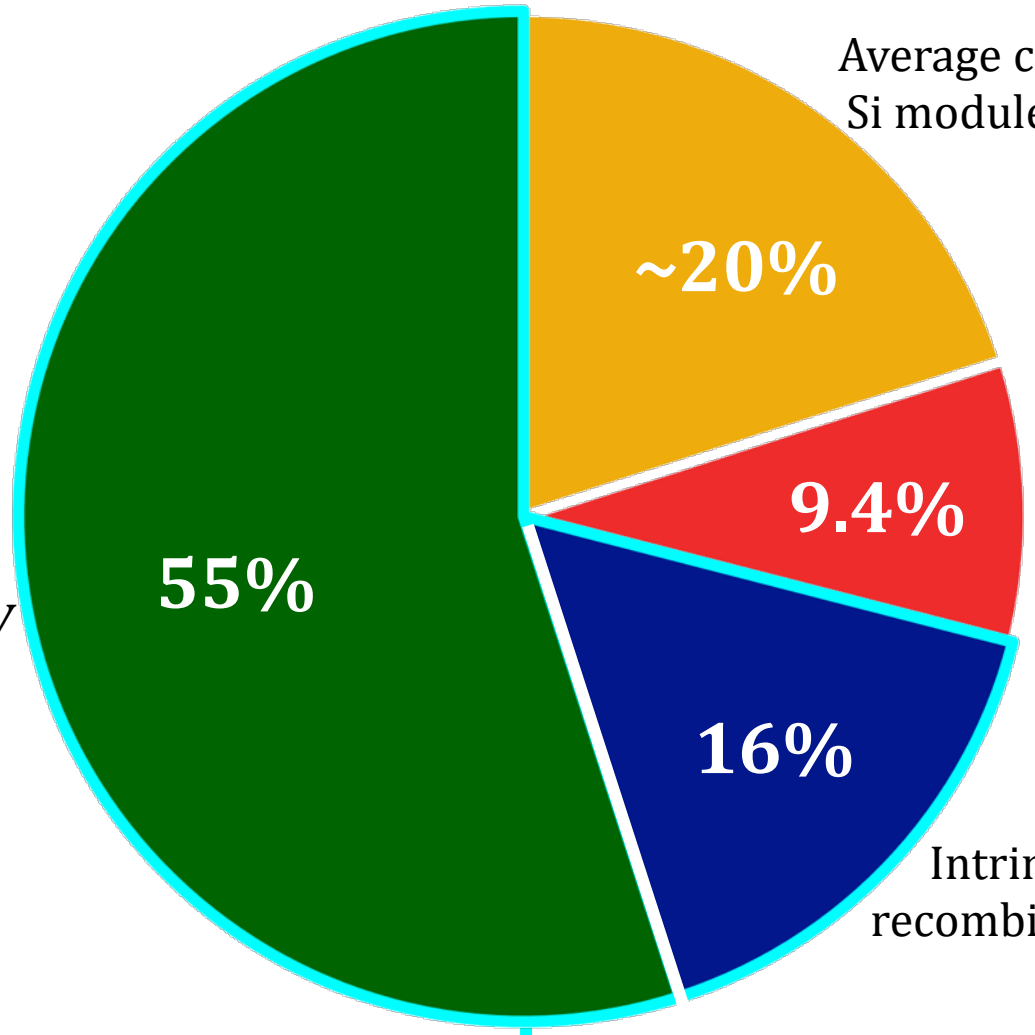

Average commercial Si module efficiency

Technological losses

- Optical
- Resistive
  - Si wafer, bulk
  - Electrode-to-wafer contact
- Defects
  - Bulk
  - Surface

-Dangling bonds

-Electrode-to-wafer interface

Intrinsic recombination

$E_{photon} < 1.11\ eV$ + Thermalization

Fundamental losses

Pie chart adapted from Dingemans, G. Ph.D. dissertation, 2011.

Highly doped *c*-Si confers charge-carrier selectivity, at a cost

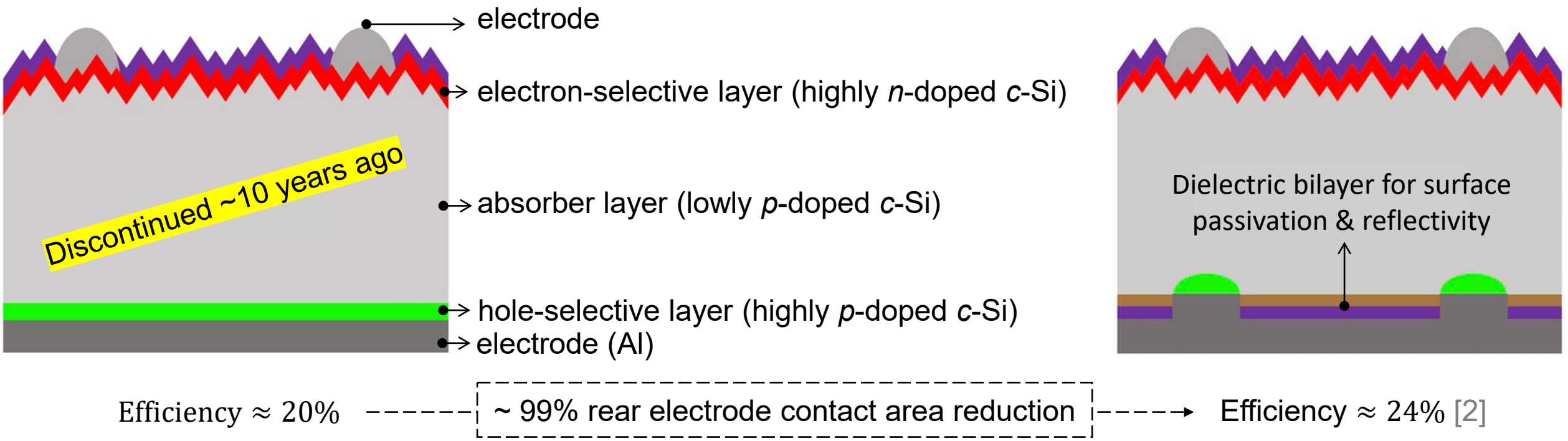

- In n^+ *c*-Si, [ē] >> [h]. This confers much higher conductivity for ē. The opposite is true for p^+ *c*-Si.
- Higher concentration of dopants in n^+ and p^+-Si enhances recombination via Auger-Meitner effect.
- Rear contact area can be reduced to maximize passivation & minimize contact resistivity, combined.

[2] Min et al. "A roadmap towards 24% efficient PERC solar cells in industrial mass production," IEEE Journal of Photovoltaics. 2017.

Charge-carrier transport mechanisms in POLO passivating contacts

Polycrystalline silicon on silicon oxide (POLO)

Efficiency ≈ 26%

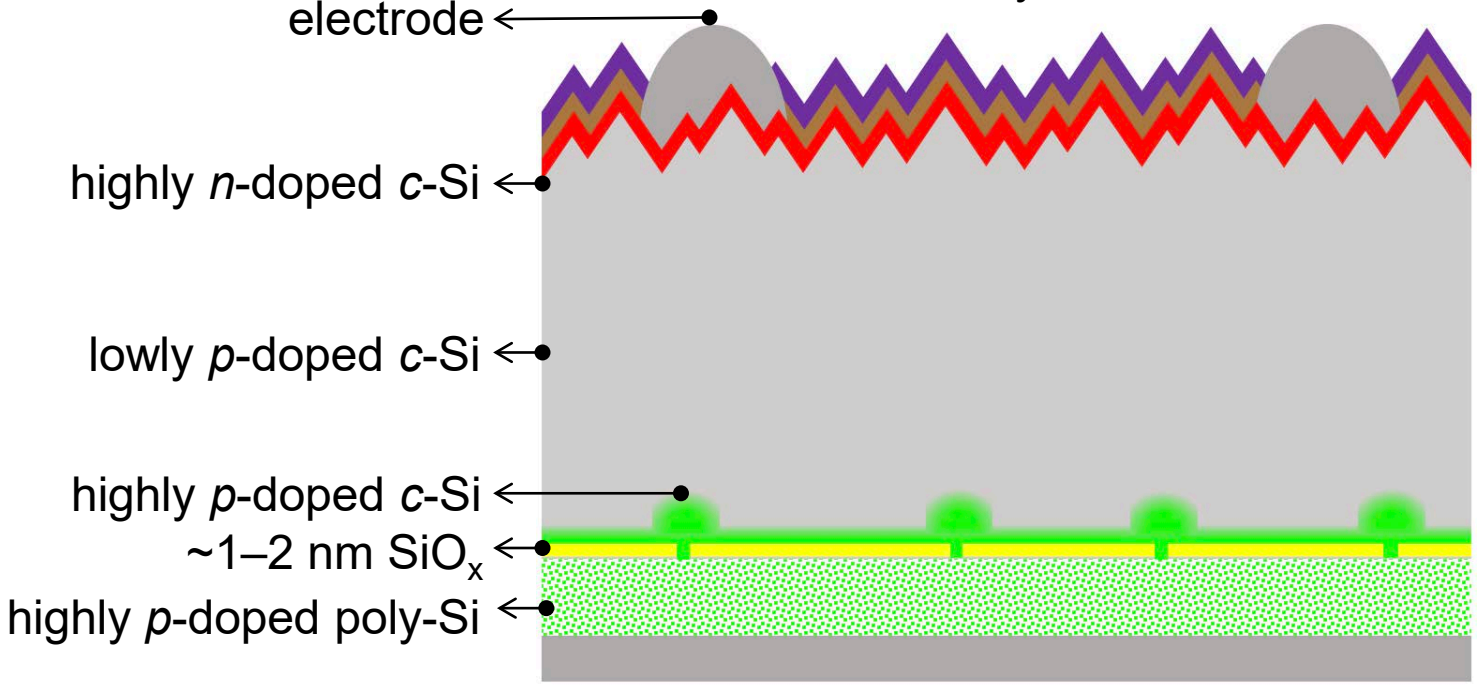

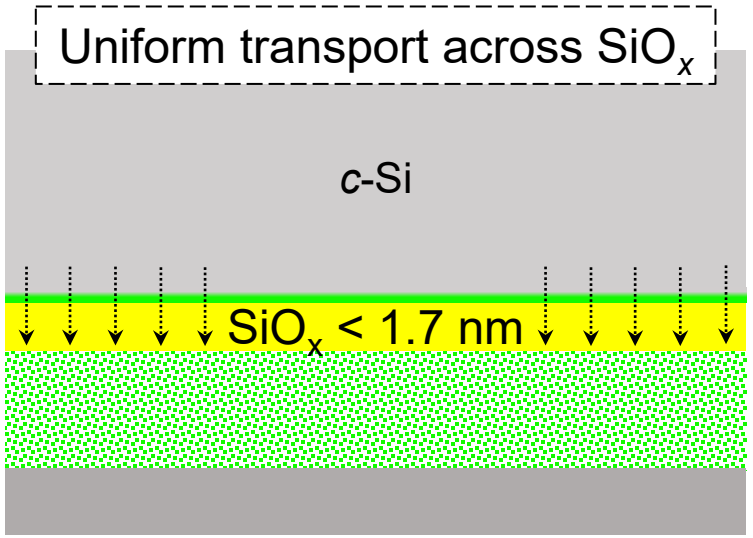

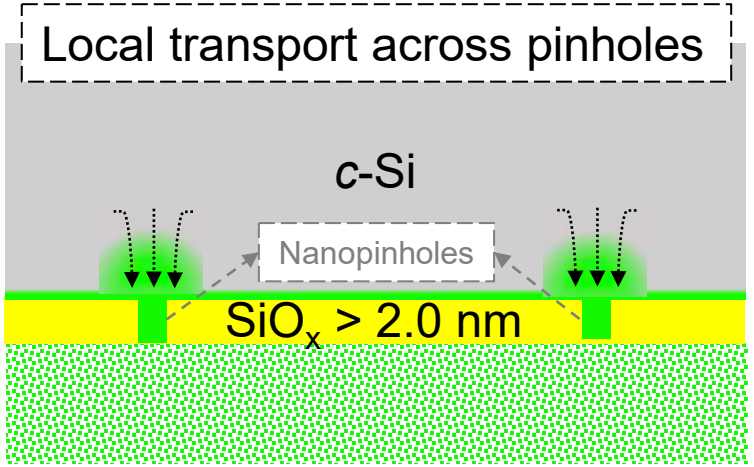

Currently, nanopinholes must be formed via thermal budgets.

SiO_x serves as barrier to further etching of the bulk *c*-Si

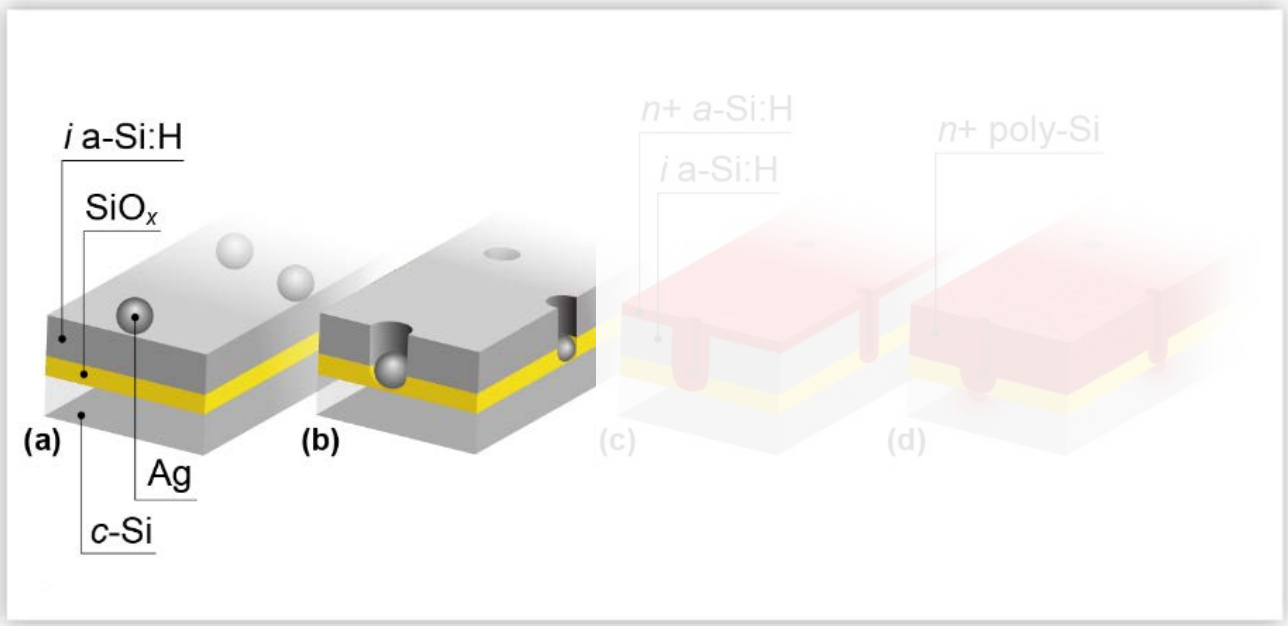

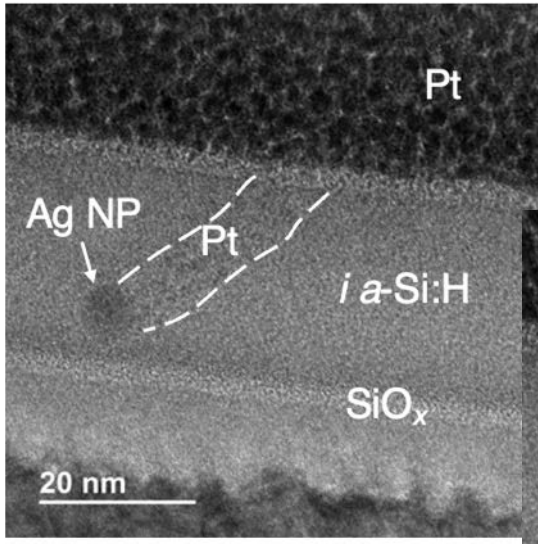

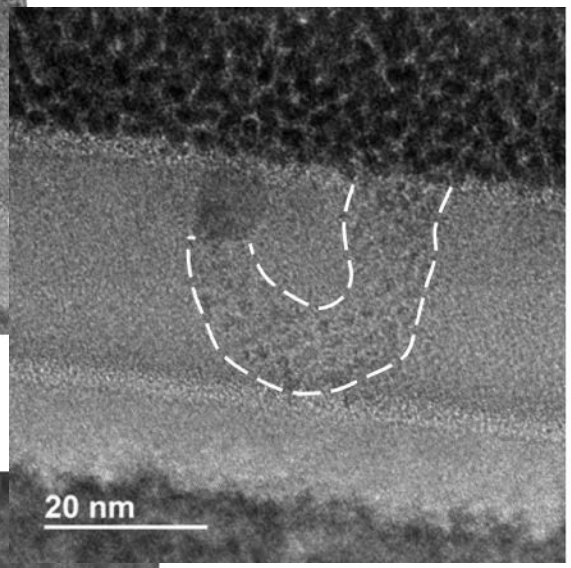

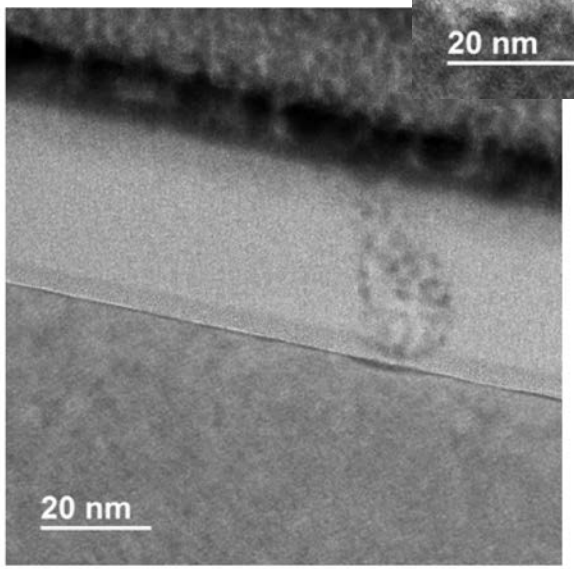

(1) Ag NP size is proportional to etching depth

(2) Not all nanoparticles create pinholes in SiO_x

(3) SiO_x serves as an effective etch “stop”

(4) SiO_x etch rate is hindered by preferential etching of *i a*-Si:H, which competitively consumes HF.

Process for PLEO and PLENO fabrication yields well-passivated contacts

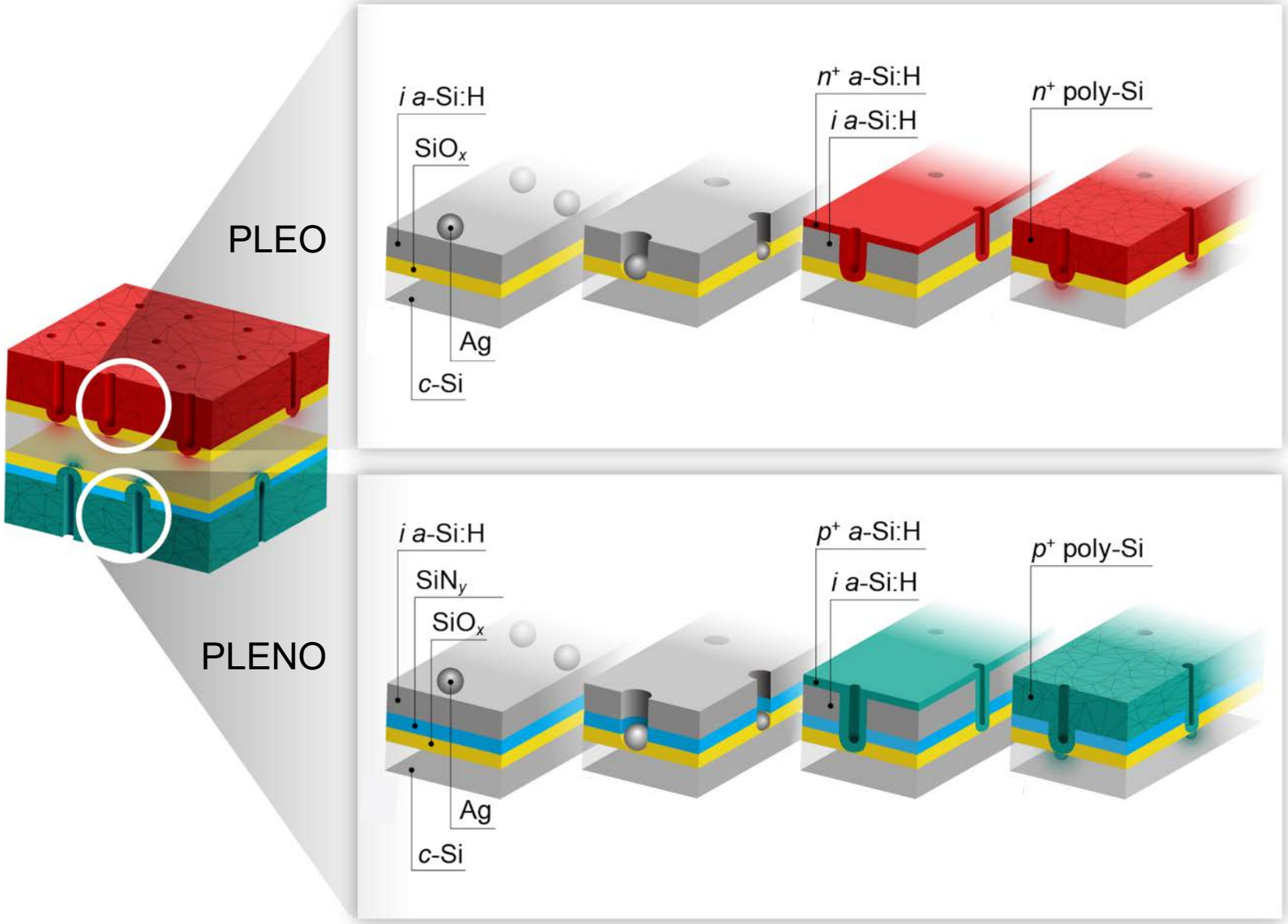

_a_-Si:H in $AgNO_{3(aq)}$

$$Ag^+ + e^- \rightarrow Ag^0$$

Ag-loaded _a_-Si:H in $HF:H_2O_{2\ (aq)}$

Electrochemical half-reactions

$$H_2O_2 + 2H^+ + 2e^- \rightarrow 2H_2O$$

$$Si + 2H^+ \rightarrow Si^{4+} + H_2 + 2e^-$$

Chemical dissolution reaction

$$Si^{4+} + 6HF \rightarrow 6H^+ + SiF_6^{2-}$$

Mesopore filling with doped _a_-Si:H

Dopant drive-in and _a_-Si crystallization into poly-Si

(not shown) hydrogenation + electrode deposition

Unfathomed n^+ PNO delamination

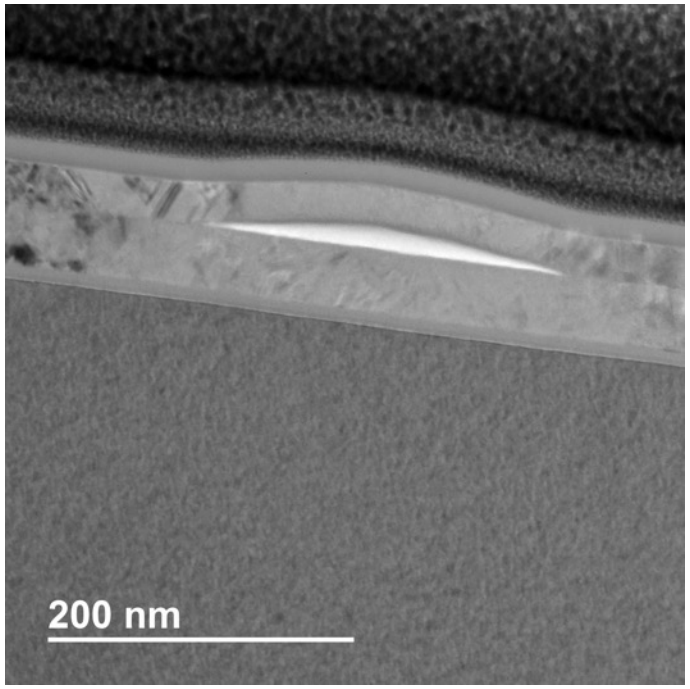

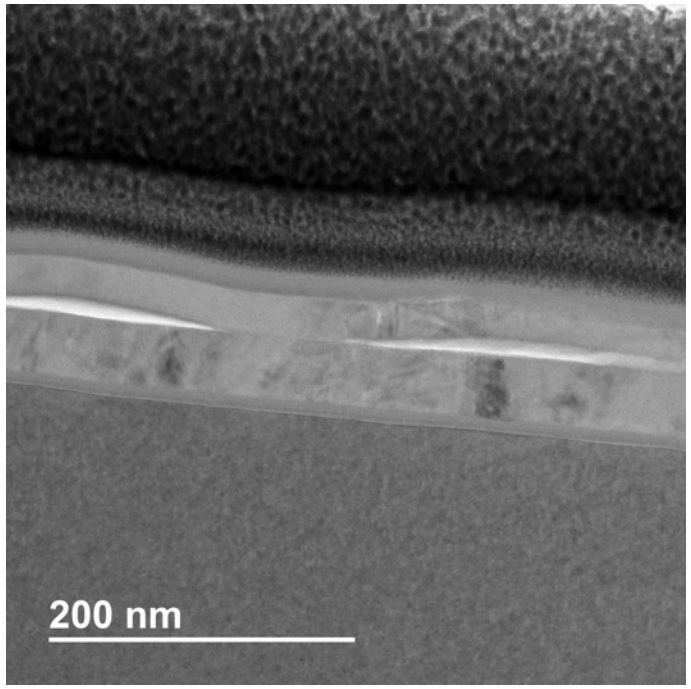

Location where delamination occurs seem to coincide with the intrinsic and n^+ doped *a*-Si:H interface (TEM is after crystallization)

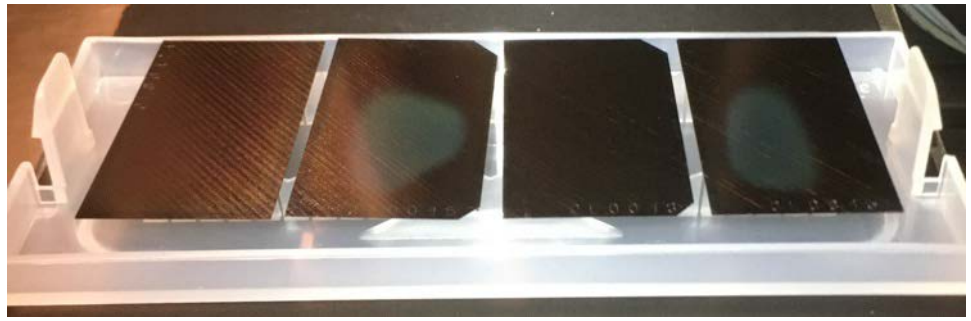

Cell gridline design + aperture mask

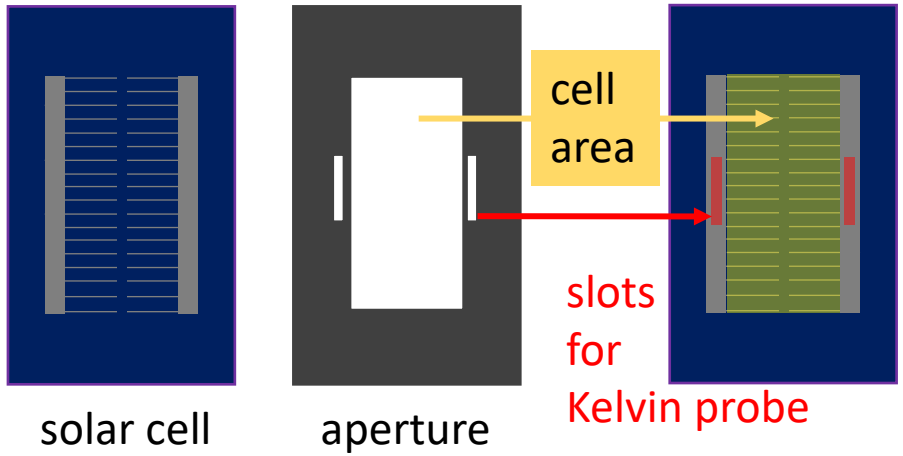

- 3 cm by 5 cm substrate
- 1.6 cm by 2.5 cm, 4 cm^2 cell
- 42 gridlines are 7.44 mm vs 27.9 μm
- Aperture mask is made of SiN_y/Al-coated Si wafer

Sinton output for champion SST cell

Exposure 1/50s

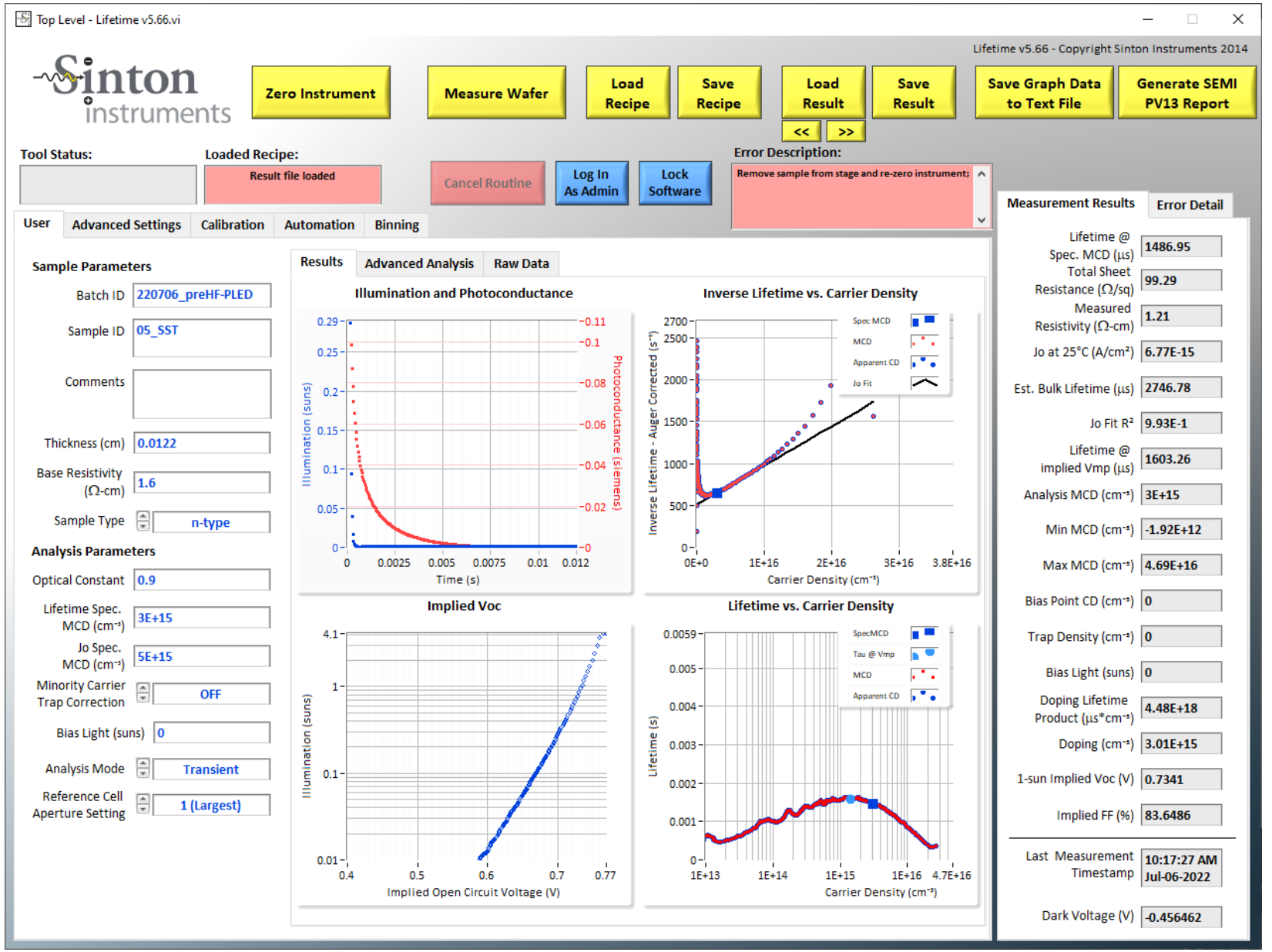

Exposure 1/25s

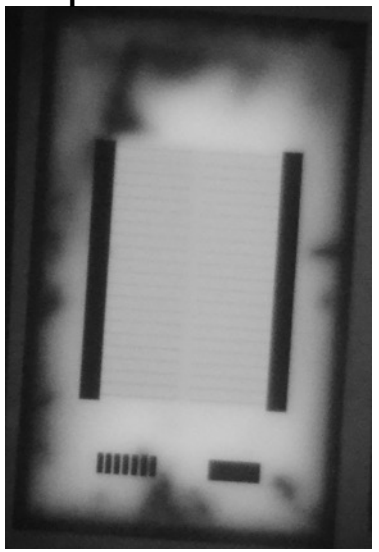

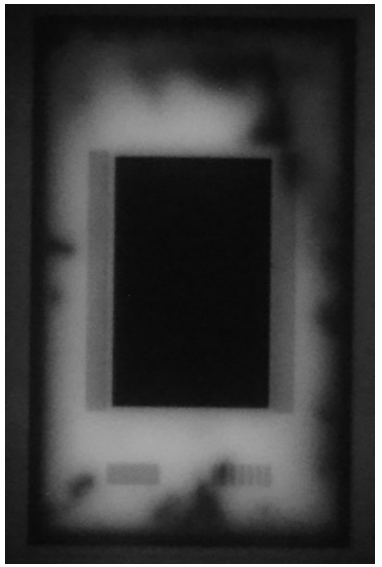

Thin film info

~2 nm SiO_x: 800 °C, 6:1 N_2:O_2

~8 nm SiN_y: SiH_4/NH_3 (4 and 24 sccm, respectively) at 200 °C, 4 W, and 0.4 Torr

Refractive index:
N-H/Si-H ratio: 0.23

~30 nm intrinsic *a*-Si:H: SiH_4/H_2 (2 and 120 standard sccm, respectively) at 250 °C, 12 W, and 1.4 Torr

~20 nm boron-doped *a*-Si:H: SiH_4/H_2/2.6% B_2H_6 in H_2 (2, 100, and 2 sccm, respectively) at 200 °C, 8W and 1 Torr

~20 nm phosphorous-doped *a*-Si:H: SiH_4/H_2/3% PH_3 in H_2 (2, 100, and 2 sccm, respectively) at 220 °C, 8 W and 1 Torr.

Doping in poly-Si: approx. 10^{20} cm^{-3}